



A review on graphene and graphene composites for application in electromagnetic shielding

Svetlana Jovanović¹ · Miroslav Huskić² · Dejan Kepić¹ · Muhammad Yasir³ · Kamel Haddadi⁴

Received: 7 September 2023 / Revised: 30 September 2023 / Accepted: 4 October 2023 / Published online: 18 October 2023
© The Author(s) 2023

Abstract

As wireless solutions for communication, information, and sensing in modern society, electromagnetic waves (EMWs) have contributed considerably to the increase in the quality of people's everyday lives. At the same time, EMWs produce electromagnetic pollution, issues with electromagnetic interference (EMI), and radio frequency (RF) signal leakage. These circumstances lead to high demand for efficient EMI shielding materials.

To design an EMI shielding product, a compromise must be achieved between the electromagnetic shielding efficiency, the thickness of shielding materials, durability, mechanical strength, reduced volume and weight, and elasticity. Due to its ability to block EMWs, flexibility, lightweight, and chemical resistivity, graphene has been identified as a promising candidate material for efficient EMI shielding. Herein, we reviewed the studies that investigated various graphene-based composites as potential EMI shielding materials, with a focus on the composites based on graphene and silver nanowires due to their high EMI shielding efficiency, low production price, and favorable mechanical properties.

Keywords Graphene · Graphene oxide · Silver nanowires · Composites · Electromagnetic interference shielding

1 Introduction

The rapid development of technology led to a large number of electronic devices used in everyday life and professionally. Smartphones and various smart gadgets became inevitable parts of modern life. These changes make our life more comfortable. All these electronic devices emit electromagnetic waves (EWs) and lead to a new form of modern contamination, named electromagnetic pollution. EWs can cause serious issues as a result of electromagnetic wave pollution

leading to electromagnetic interference (EMI), and information leakage. Devices that generate EMI are those that transmit, distribute, or use electric energy. When EWs penetrate between equipment joints, they can affect the performance of different devices, lead to damage to instrument components, and eventually reduce the device's lifetime. EMI could also be dangerous for people with pacemakers and implantable cardioverter–defibrillators (ICDs) [1–3]. Particularly important is professional exposure to radiofrequency (RF) electromagnetic fields. Power plant workers, those operating on medical instruments, workers in the metal industry, on welding machines, and in telecommunication are exposed to this type of electromagnetic field. Extremely low-frequency electromagnetic fields (ELF EMFs frequency < 300 Hz) are ubiquitous. Surprisingly, their effects on living organisms are poorly understood and subjected to debate.

Several studies linked the risk of childhood cancer, particularly leukemia, to ELF EMF exposure [4–7] and brain cancers such as glioma [4]. Chronic exposure leads to changes in neuronal activity, affects long-term potentiation in hippocampal CA1 region, and shows an inhibitory effect on the amplitude of long-term potentiation [5]. These changes indicated that ELF EMF affects learning and memory. Other studies associate ELF EMF with sleep quality,

✉ Svetlana Jovanović
svetlanajovanovic@vin.bg.ac.rs

¹ Vinča Institute of Nuclear Sciences-National Institute of the Republic of Serbia, University of Belgrade, P.O. Box 522, 11000 Belgrade, Serbia

² Faculty of Polymer Technology, Ozare 19, 2380 Slovenj Gradec, Slovenia

³ Carl Von Ossietzky Universität Oldenburg, 26111 Oldenburg, Germany

⁴ CNRS, Centrale Lille, Univ. Polytechnique Hauts-de-France, UMR 8520 - IEMN - Institut d'Electronique de Microélectronique et de Nanotechnologie – Lille, Univ. Lille, 59650 Villeneuve-d'Ascq, France

anxiety, and depression [6]. The study where 66 scientific publications were analyzed using a meta-analysis of observational studies in epidemiology (MOOSE) concluded that chronic exposure to EMFs elevated the risk for neurodegenerative diseases (amyotrophic lateral sclerosis and Alzheimer's disease) by 10% [7]. Other studies showed that ELF EMFs induce stress reactions, causing morphological as well as physiological alterations in subjected organisms [8]. Occupational exposure to ELF EMFs was not connected to an increased risk of malignant lymphoma [9]. Jalilian et al. analyzed the cases of different lymphoma registered between 1961 and 2005 in Finland, Iceland, Norway, and Sweden, and the prevalence was similar to the population that was not exposed to ELF EMFs. While short-term exposure does not affect cortisol levels in humans [10, 11], its secretion pattern is changing and it is related to the field intensity in the case of long-term exposure [12]. As a major glucocorticoid hormone, cortisol level was followed in the blood of workers occupationally exposed for 1–20 years. This study revealed a change in the cortisol secretory pattern. The suppressive effect of ELF EMFs on the levels of chromogranin A, a marker of neuroendocrine tumors and stress, was also reported [13]. Scientists are disagreeing regarding the effects on human health, due to a lack of clear cause–effect connection. But ELF EMF certainly contributes to ROS production and oxidative stress and many other diseases [14].

Thus, the need for materials that can protect people but also instruments from both EWs and interference is increasing along with technological development. Material with EMI shielding efficiency (EMI SE) of 20 dB is appropriate for commercial applications. Thick and dense conductive materials are efficient in EMI shielding. A highly effective EMI shielding material is metal. But, metals in the form of foil or fibers are rigid, with poor elasticity, they are not transparent, not good for wearable applications, and they reflect EWs leading to further secondary EWs pollution. Another material is conductive polymer composites (CPCs), which are lightweight, have good sealability, are easy to mold, are relatively low cost, and have no magnetic interference [15–17]. Silicone rubber also showed a good EMI performance due to excellent high- and low-temperature stability, weather, and chemical resistance [18, 19].

For the use in EMI shielding, the new material should be lightweight, thin, elastic, durable, flexible, chemically stable, economically acceptable, produced by eco-friendly procedure, and resistive to moisture, in order to be applicable in the space and aircraft industry, motor vehicles, portable and wearable electronic devices.

One of the promising materials for EMI shielding is graphene, its derivatives, and composites. Due to its flexibility, lightweight, electrical conductivity, and chemical resistivity, graphene attracted large attention as a shielding material [20]. Graphene was discovered by Geim and Novoselov

using adhesive tape to mechanically exfoliate graphite and isolated graphene for the first time in 2004 and won a Nobel prize in 2010 for this discovery [21]. From high-quality graphene produced by chemical vapor deposition (CVD), electrochemically exfoliated graphite, to more defective graphene with poorer electrical conductivity produced by the reduction of graphene oxide, graphene showed different properties as well as cost. In this review, we will analyze graphene produced using different methods, and its composites for application in EMI shielding addressing the most promising approaches to achieve desired shielding efficiency (SE), considering both economic and ecological aspects of production. Due to the volume of the work published in the field of electromagnetic shielding, we restricted our study to graphene, considering the rising interest in this material in EMW shielding. This field has evolved drastically in the last decade, which creates a need for comprehensive but clear studies understandable for researchers across different fields. A large number of review papers are analyzing MXene, conductive polymers, and graphene-based composites, while only a few review papers explore graphene as EMI shielding material [22–24]. In contrast, this review paper focuses on the EMI shielding of graphene and connects its structural characteristics with measured SE, and to composites with silver nanowires which greatly contribute to the efficiency of graphene sheet to block EMWs.

2 EMI shielding

EM shielding is based on reflection, absorption, and multiple reflections [25, 26]. Shielding efficiency describes how well materials block EMWs and it is expressed in decibels—dB. Higher values of dB mean that material is more efficient in EMI shielding. The commercial application requires a minimum SE of 20 dB, which is equivalent to the blocking of 99% of incident EMWs.

The total shielding efficiency (SE_T) of a material is the sum of reflection (SE_R), adsorption (SE_A), and multiple reflections (SE_{MR}) shielding. EMWs are characterized by power (P), electric (E), and magnetic field (H) intensities. Thus, SE_T is defined as the logarithmic ratio of the incident (P_i) to transmitted power (P_T) of electromagnetic radiation according to the following relations (1) and (2):

$$SE_T = 10 \log \frac{P_i}{P_T} = 20 \log \frac{E_i}{E_T} = 20 \log \frac{H_i}{H_T} \quad (1)$$

$$SE_T = SE_A + SE_R + SE_{MR} \quad (2)$$

where I —indicated incident, R —reflected, and T —transmitted component of EWs [27]. The interaction of the EM waves in the collision with different EMI shielding materials

is described in Fig. 1, where reflection, absorption, and multiple reflections are presented.

Electrically conductive materials such as metals are mainly reflecting EWs when they hit the surface rich in electrons and the SE_R is related to the ratio between the conductivity (σ) and permeability (μ) of the material, according to Eq. 3.

$$SE_R = 39.5 + 10 \log \frac{\sigma}{2f\pi\mu} \propto \sigma/\mu \tag{3}$$

While reflection is primary, the absorption of EMWs is a secondary mechanism of EM shielding. Materials with magnetic or electrical dipoles are candidates for absorption shielding which is related to the following equation:

$$SE_A = 20 \log \frac{d}{e^\sigma} = 8.7d\sqrt{f\pi\sigma} \propto d\sigma\mu \propto ad \tag{4}$$

where d is the thickness, and α is the attenuation constant of the slab, respectively. For magnetic conductive materials, absorption is the dominant shielding mechanism and it is directly proportional to the permittivity of the materials [27].

The multiple reflection is the process during which EW undergoes multiple internal reflections due to inhomogeneity and occurs between the interface layers [28, 29]. This type of shielding is characteristic of thin materials and happens when EWs are trapped inside the boundaries of materials, where they have reflected again from one to another boundary. The SE_{MR} can be calculated using the following expression:

$$SE_{MR} = 20 \log \left(1 - e^{-\frac{2d}{\delta}} \right) \tag{5}$$

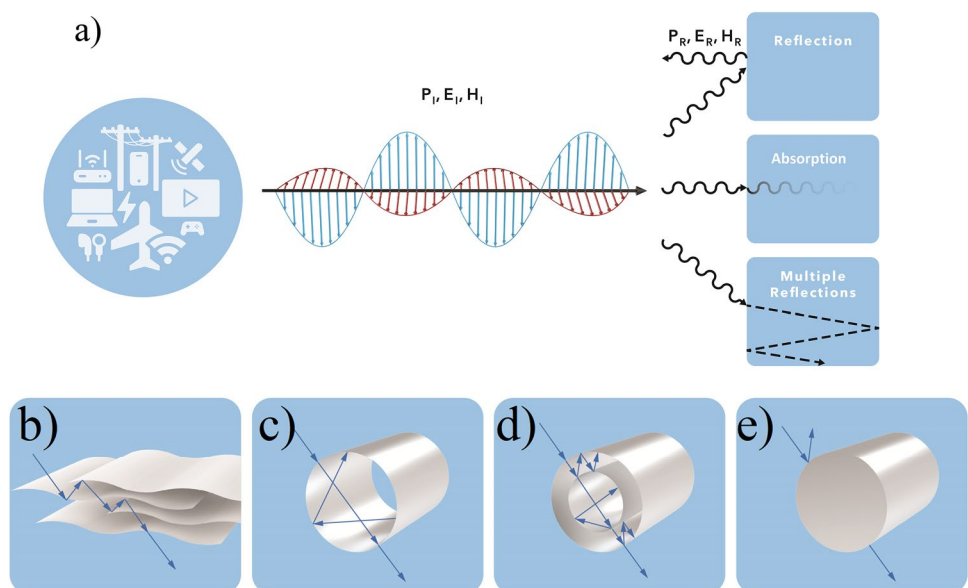
where d is the sample thickness and δ is the penetration depth. This type of shielding is observed in porous structures, where hollows in the internal structures become active

spots for the scattering of EMWs and make SE_{MR} similar to the absorption of EMWs. The schematic presentation is shown in Fig. 1b.

The most desirable shielding mechanism is absorption, considering that EMWs in that case were not emitted back into the environment. The higher the dB level of EMI shielding effectiveness, the less energy is transmitted through the shielding material. In EMI shielding theory, when an EM wave impinges on a shielding material, the incident power is divided into reflected, absorbed, and transmitted power and the corresponding power coefficients of absorbance (A), reflectance (R), and transmittance (T) are such that $R + T + A = 1$. The fraction of the absorbed EMWs is calculated from the previous equation, $A = 1 - R - T$. In a vector network analyzer (VNA), scattering parameters S_{11} (or S_{22}) and S_{21} (or S_{12}) are measured to calculate the reflectance and transmittance power coefficients, $R = S_{11}^2$ and $T = S_{12}^2$, and the absorbance is indirectly derived from $A = 1 - R - T$. Apart from these coefficients, to evaluate the efficiency of EMI shielding materials, the values of two more parameters were considered: specific EMI shielding effectiveness (SSE) and absolute effectiveness (SSE/thickness of material).

In the recent past, graphene has become an interesting shielding material due to its electrical properties such as high electrical conductivity, and saturation velocity, good mechanical properties such as flexibility and strength, but also resistivity to corrosion and chemical reagents. Thus, in only the last 5 years the interest in graphene as EMI shielding materials largely increased (Fig. 2). Results of searching the Scopus database using keywords “electromagnetic interference shielding” and “graphene” showed that in 2022 was 262, while just 10 years ago, the number of papers published with the same keywords was only 11.

Fig. 1 Interaction of EMWs with materials, absorption, transmission, and multiple reflections (a). EW inside of lamellar materials (b), porous (c, d), and compact materials (e)



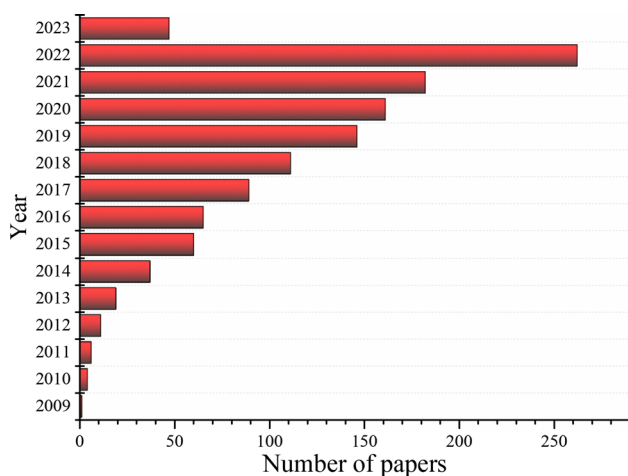


Fig. 2 Results of the Scopus database on 1st February 2023, using TITLE-ABS-KEY “electromagnetic interference shielding” AND “graphene”

Composites based on graphene oxide and silver nanowires (AgNWs) were not explored widely as electromagnetic shielding material although they seem like a very efficient shielding material with good mechanical properties and chemical inertness. Table 1 summarizes the morphology of graphene and AgNWs, electrical conductivity and sheet resistance, and EMI SE values for different composites. Results indicated that GO alone as well as in composite with AgNWs produces a good shielding barrier. In the further part, we are exploring structural properties as well as the mechanism behind the shielding effects of these nanomaterials.

2.1 Graphene and graphene oxide, from structure and properties to application in EMI shielding

2.1.1 Graphene analysis

Graphene is a 2D nanomaterial composed only of C atoms that are sp^2 hybridized. C atoms are organized in the 6-membered so-called benzene ring. Each atom is covalently bonded to three neighboring carbons, which leaves one unpaired electron per each C. Orbitals of these unpaired ones are overlapping creating a π -cloud above and over each ring, while in graphene, these clouds from each benzene ring create a unique cloud where electrons traveling freely. This structure makes graphene a unique material considering its electrical, mechanical, thermal, and chemical properties [46]. To study these mostly sp^2 structures and their derivatives such as graphene oxide, the most important techniques are Raman, Fourier Transform infrared, X-ray photoelectron spectroscopy, X-ray diffraction, and others [47–56]. Typical Raman, XPS, FTIR, and XRD spectra of graphene and its oxidized derivative, GO are presented in Fig. 3. In the Raman

spectrum of graphene (Fig. 3a), the most intense band is the so-called graphitic or G band which stems from in-plane stretching of sp^2 bonded C atoms, it is located usually around 1585 cm^{-1} [57, 58], while the 2D band is the second-order overtone of the G band and its intensity and shape are related to the number of the graphene layers, as presented in the left part of Fig. 3a showing deconvolution of 2D band and estimation of layers numbers [47]. In the Raman spectra of GO, an additional band around 1380 cm^{-1} is present (defect or D-band) and its intensity is correlated with defects in graphene structure such as edges, heteroatoms, vacancies, and Stone-Wale [59–62]. The ratio between the intensity of D and G bands (I_D/I_G) is proportional to the level of structural disorder and it is 0 for defect-free graphene and from 0 to above 2 for highly defective structures such as GO [62]. The shoulder bands in the Raman spectra of the GO located around D and G bands can be identified by spectral deconvolution [50], and their position is dependent on the oxygen content in GO or reduced GOs, as presented in Fig. 3b.

Typical wide-scan XPS spectra of graphene oxide show peaks from C and O 1s [64–66], while analysis of those reveals the at% of each functional group in materials [48]. In Fig. 3b, the removal of oxygen-containing function groups at different temperatures can be observed as an increase in at% of sp^2 C atoms, and lowering of C–OH, C–O–C, C=O/HO–C=O, and C=O, as well as the enhancement in the C/O ratio presented in the upper right corner. FTIR spectra are often used to identify the presence of functional groups, but it does not give quantitative data about their content [67, 68]. Band assign to carboxyl (–COOH) is usually around 1020 cm^{-1} , epoxy (C–O–C) at 1243 cm^{-1} , aromatic sp^2 (C=C) at 1544 cm^{-1} , 1627 cm^{-1} from carbonyl (C=O), and from hydroxyl (–OH) groups band is located at 3420 cm^{-1} [68]. XRD is a valuable tool to investigate graphene-like structures and one example is presented in Fig. 3e. Graphite shows only one sharp peak at $2\theta = 26.4^\circ$ which corresponds to the (002) diffraction plane [69–71] and the lattice distance of 0.34 nm. Oxidation leads to an increase in the interlayer distance due to layers exfoliation, water intercalation, and incorporation of functional groups on the basal plane of graphene sheets and this could be observed by shifting the peak to a lower angle, to 10.9° which corresponds to layer distance of 0.81 nm [49]. When GO is reduced, the peak 2θ is shifting to higher angles, while declining in the interlayer distance could be used to follow the process of reduction as well. This can be seen in Fig. 3e, where GO loses functional groups over time of the hydrothermal reduction treatment and the graphene structure has been partially restored.

The morphology of the graphene and graphene oxide is usually studied using atomic force microscopy (AFM) which gives information about surface roughness, sheets size, sheets height, and profiles (Fig. 4a–h) [72, 73]. By measuring the height of the sheet using AFM, the number

Table 1 Summarized results of various graphene-based nanomaterials, and their electrical (sheet resistance, R and electrical conductivity, σ), structural properties, and EMI SE

Material	Graphene or GO	AgNWs ^a	R or σ	Structure	EMI SE
Graphene oxide (GO) films [30]	Hummer's ≈ 1.1 nm thick 1.2 μm	–	1000 S/cm	XPS C/O 73.1; XRD: 26° (002), I_D/I_G 0.14	20 dB
Graphene oxide [31]	Hummer's Small SGO 1 μm^2 Large LGO 23 μm^2	–	152 ± 7.5 S/cm	XPS: C/O 1.79 (rSGO) to 6.75 (rLGO); I_D/I_G 0.9–1.4 XRD: (002)	
AgNW/cellulose papers [32]	–	Polyol D 19 nm L 18 μm	67.51 S/cm	XRD: (101), (002), (111), (200), (220), (311)	48.6 dB at 1 GHz
GO/AgNWs/GO films [33]	Hummer's	D 15–35 nm L 15–25 μm	6.5×10^4 S/m	XPS C/O: 9 Raman I_D/I_G 1.4	38 dB at 8.4–12 GHz
PET/AgNWs/Graphene [34]	CVD graphene	D 90 nm L 40 μm	199.75 to 152.33 Ω/sq	–	–
rGO/AgNWs composites on glass, textile fabric, and PET [35]	High shear speed of expanded graphite 3–15 layers 10 to 30 μm	Polyol D 30–50 nm L 30–50 μm	6–24 Ω/sq	XRD: (002), (111), (200), (004), (220) XPS O/C 0.041 contact angle: 129	–
PET/AgNWs/GO/acrylic NP [36]	0.5–5 μm	D 35–45 nm L 5–15 μm	34.8 Ω/sq	Contact angle 86.3°	20 dB (0.5–3 GHz)
GO/AgNWs composite [37]	40 μm	$D \sim 37$ nm $L < 10$ μm	2.9×10^6 S/m	density 2.9 g/cm ³	92 dB for 2.9 g/cm ³ , 32 dB for 18 μm on cotton
G/GQDs/AgNP in PVDF [38]	Improved Hummers			XRD: (111), (200), (220), (311)	43 dB at 8 GHz
GO/AgNWs/PDMS aerogel [39]	Hummer's	Polyol	12.1 S/cm		34.1 dB
Polyurethane/GO/AgNW [40]		D 20–25 nm L 25–30 μm			20 dB
PET/GO/AgNWs/Ag grids/PET [41]		Polyol	1.6 Ω/sq	Transparency 74.4%	42.9 dB at 1.8 GHz
rGO/AgNWs aerogels [39]	5–8 μm	D 60 nm L 20–30 μm		XPS C/O 6.6, I_D/I_G 1.6, XRD: (002), (111), (200), (220), (311)	45.2 dB
PMMA/graphene/metal mesh hybrid [42]			5.53 Ω/sq		28.9 dB at 12–18 GHz
AgNWs/GO [43]				XRD: (002) GO, (111), (200), (100)	40.1 dB
AgNWs/GO [44]				I_D/I_G : 1.1–0.7, XPS: O groups, XRD: 25–46 nm	35.5 dB
Free-standing GO–AgNW composite [45]	0.5–2 μm size	D 40 nm L 20–45 μm	1144.32 to 2255.8 S/cm	Charge of GO: –47.4, Ag NWs: +16.2 mV XRD: (001), (111), (200), (220), XPS C/O 0.33–0.37	55.16 dB 66 779.66 dB cm ⁻¹

^a D is diameter, L is length

of graphene layers could be estimated (Fig. 4b, d) or it can show the surface roughness of the sheet which is usually related to functional groups (Fig. 4g, h). Scanning electron microscopy (SEM) is used for the investigation of the cross section morphology of the standing films and the film thickness (Fig. 4i, j) [74–76] but also for analysis of sheet morphology (Fig. 4k, l) [77–79]. Transmission electron

microscopy (TEM) is an inevitable tool for the analysis of sheets size, and layers numbers (Fig. 4m, n, o) [80]. It even offers the possibility to investigate graphene structure at the atomic level and contributes to the estimation of the presence of defects such as vacancies (Fig. 4n) or to study edges (Fig. 4o). Apart from microscopic techniques, methods such as dynamic light scattering (DLS) [81] and zeta sizer are

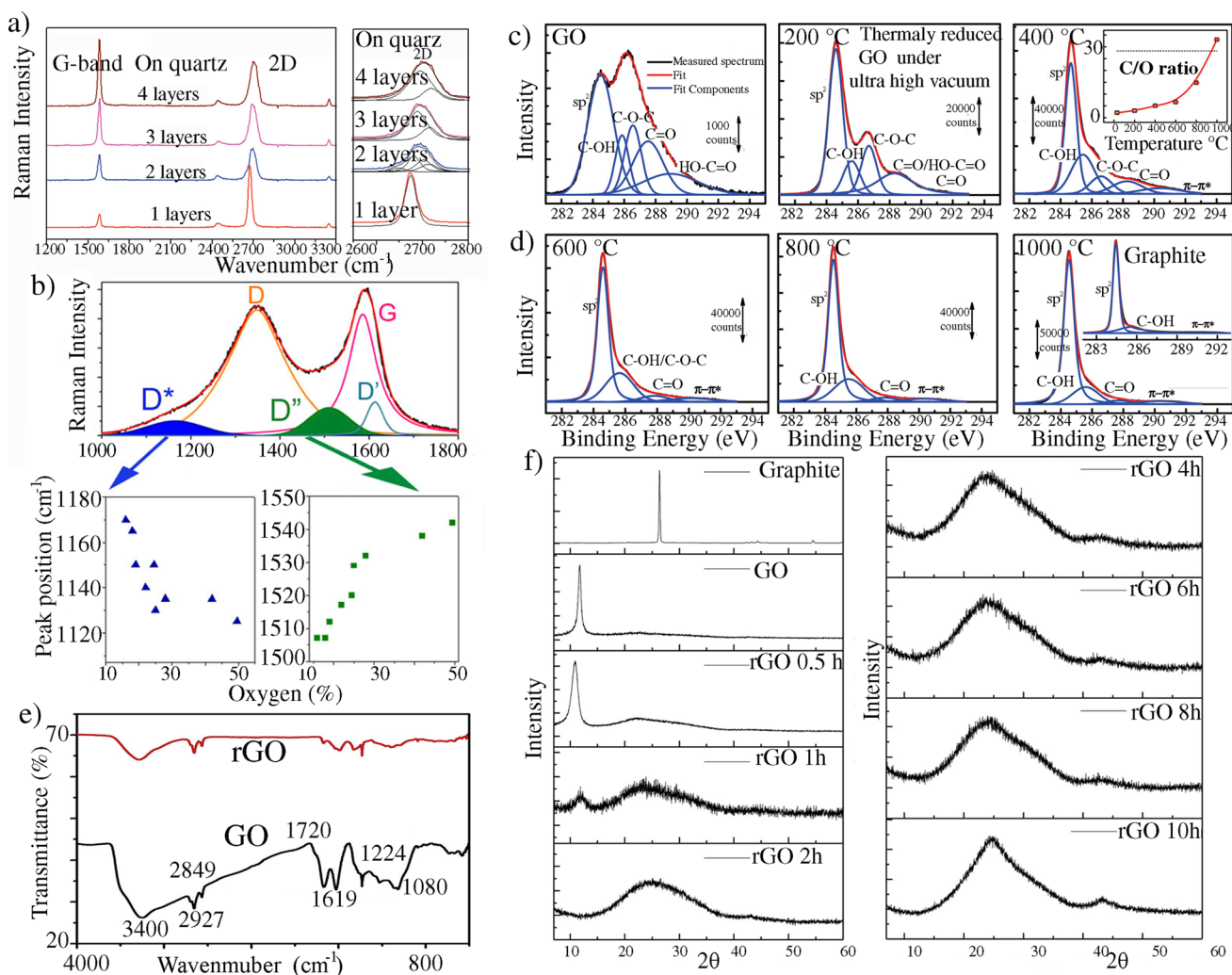


Fig. 3 Raman spectra of graphene (a), reprinted with permission from Raman Studies of Monolayer Graphene: The Substrate Effect, by Yingying Wang, Zhen Hua Ni, Ting Yu, et al., *The Journal of Physical Chemistry C*, 112, 29, 10,637–10640, Copyright 2008 American Chemical Society [47], and graphene oxide (b) reprinted with permission from The Importance of Interbands on the Interpretation of the Raman Spectrum of Graphene Oxide by Sergi Claramunt, Aida Varea, David López-Díaz, et al., 2015, 119, 18, 10,123–10129, Copyright 2015 American Chemical Society [51], XPS from (c and d) reprinted with permission from Probing the Thermal Deoxygenation of Graphene Oxide Using High-Resolution In Situ X-ray-Based Spectroscopies by Abhijit Ganguly, Surbhi Sharma, Pagona Papakonstantinou, et al., 2011, 115, 34,

17,009–17019, Copyright 2011 American Chemical Society [48], FTIR spectra of rGO and GO reprinted with permission from Controlled synthesis, characterization and reduction of graphene oxide: A convenient method for large-scale production by Tarko Fentaw Emiru, Delele Worku Ayele *Egyptian Journal of Basic and Applied Sciences* 4, 1, 2017, 74–79, Copyright Creative Commons Attribution-NonCommercial-NoDerivatives License (e) [50], and XRD spectra of graphite, GO and reduced GO at different condition, reprinted from Structural Evolution of Hydrothermally Derived Reduced Graphene Oxide, Hsin-Hui Huang, K. Kanishka H. De Silva, G. R. A. Kumara, Masamichi Yoshimura, *Scientific Reports*, 8, Article, 6849 (2018) a under a Creative Commons Attribution 4.0 International License (f) [49]

particularly useful for investigating the average sheets size and charge of the GO in solution, respectively [82].

With numerous astonishing structural, chemical, physical, and mechanical properties, graphene attracted attention across various scientific fields [84–88]. Recently, the interest in its potential application in EMI shielding is growing. First, we will summarize the results regarding graphene, graphene oxide, and doped graphene, and after we will deal with composites with graphene and silver nanowires.

2.1.2 EMI shielding with graphene-based materials

One of the first studies reporting the ability of the graphene-based composite to block EMW was published in 2009 [89]. Liang et al. produced a composite based on GO and epoxy polymer using an in situ polymerization. GO was produced using the modified Hummer's method, followed by chemical reduction with hydrazine leading to the production of rGO. Then, the epoxy polymer was obtained directly on the

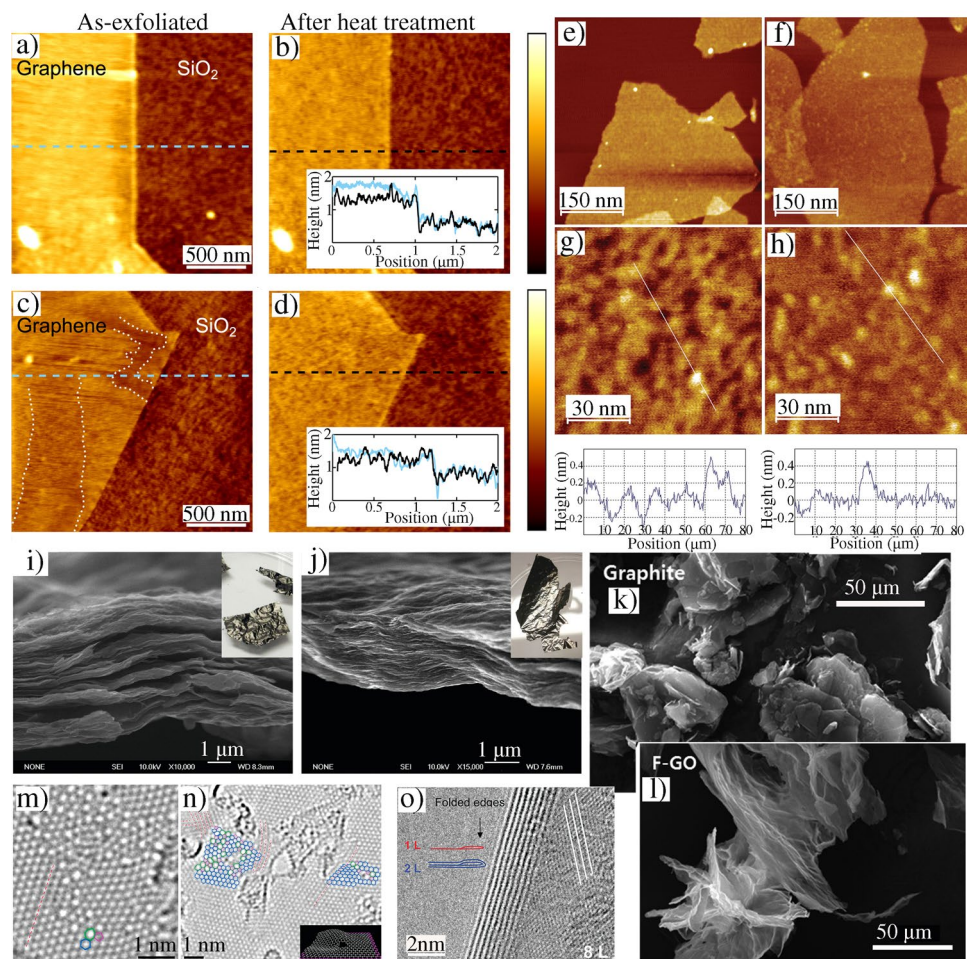


Fig. 4 AFM images of the graphene deposited on SiO₂ support before and after thermal reduction (**a–d**) adapted under the terms of the Creative Commons Attribution 3.0 license, by Lene Gammelgaard, José M Caridad, Alberto Cagliani, David M A Mackenzie, Dirch H Petersen, Timothy J Booth, Peter Bøggild Graphene transport properties upon exposure to PMMA processing and heat treatments, *2D Materials* 1 (2014) 035005. <https://doi.org/10.1088/2053-1583/1/3/035005> [73], AFM images of unreduced (**e, g**) and reduced GO (**f, h**), adapted with permission from *Langmuir* 2009, 25, 10, 5957–5968. Copyright 2009 American Chemical Society [72]; SEM images of air-dried rGO (**i**) and vacuum-annealed rGO (**j**), adapted with permis-

sion from *ACS Nano* 2010, 4(7), 3845–3852, Copyright 2010 American Chemical Society [74]; SEM image of graphite flakes (**k**) and exfoliated GO sheets (**l**) under the terms of the Creative Commons CC BY license, Copyright © 2018, Samar Azizghannad et al., Step-wise Reduction of Graphene Oxide (GO) and Its Effects on Chemical and Colloidal Properties, *Scientific Reports*, 2018, **8**, 10,083 [83]; high resolution-TEM images of GO (**m, n, and o**) adapted from adapted with permission from *Nano Letters* 2010, 10, 4, 1144–1148 by Cristina Gómez-Navarro, Jannik C. Meyer, Ravi S. Sundaram, et al. Copyright 2010 American Chemical Society [80]

graphene surface and cured. rGO/polymer composite with 15 wt% of rGO had SE of 21 dB in the frequency range between 8.2 and 12.4 GHz (X-band). Another study proved the EMI shielding efficiency of graphene, where SE was 35 dB in the frequency range of 0.1–15 GHz [90]. They showed that the electrical conductivity of graphene could be tuned by electrostatic or magnetostatic bias revealing its potential application in EMI SE.

The graphene monolayer produced using the CVD method showed a rather low EMI SE of 2.27 dB, and the main shielding mechanism was concluded to be absorption [91]. The high sheet resistance of 635 Ω/sq indicated

that monolayers had a defective structure and showed very poor SE, while those with 2 and 3 layers showed SE of 4.13 and 6.91 dB, respectively, in the frequency range of 2.2–7 GHz. With the increase in graphene layer number, the absorption component is lowering while the reflection one is increasing, which is similar behavior that was observed in thin metal films, such as Au film. Defect-free graphene was proven to be better in EMI SE than those with defects, while SE increases with the number of graphene layers [92]. When few-layer graphene was produced using the same method, the thickness of the graphene sample was 4 nm, EMI SE was 19.1 dB (18–26.5 GHz),

and transmittance was 80.5% [93]. With an increase in the electrical conductivity of graphene, i.e., multilayered graphene, a higher electrical conductivity was achieved as compared to monolayer graphene leading to higher reflection and vice versa. But, due to restrictions in the size of CVD-produced graphene, this method is inappropriate for transfer to large-scale, technically complicated, and uneconomical, thus other approaches must be considered. Graphene for application in EMI shielding is usually produced as a bulk material, using Hummer's method in the form of graphene oxide followed by reduction. The schematic presentation of the single-layered graphene structure and EM shielding is presented in Fig. 5.

Due to the presence of the discontinuities in the π -cloud, EWs are able to pass through graphene, while a part of the waves is absorbed and converted into heat. In the case of a few-layer graphene, better shielding efficiency

could be explained by multiple absorptions of the transmitted waves, as presented in Fig. 6.

When GO films were fabricated by direct evaporation of GO suspension under mild heating, it was noticed that the material possess a high EMI SE [30]. Ultrathin GO films ($8.4 \mu\text{m}$) were annealed at $2000 \text{ }^\circ\text{C}$ and showed excellent EMI shielding effectiveness of 20 dB and high in-plane thermal conductivity of $1100 \text{ W m}^{-1} \text{ K}^{-1}$. The material had excellent mechanical flexibility and structural integrity during bending, indicating that the graphitization of GO film could be considered a new alternative way to produce excellent EMI shielding material.

Chemically reduced graphene thin film had a similar EMI SE, of around 20 dB [31]. GO flakes were obtained by Hummer's method and separated into large (LGO, with a surface area of $23 \mu\text{m}^2$) and small GO flakes (SGO, area $1 \mu\text{m}^2$) by centrifugation. Free-standing films were produced

Fig. 5 Schematic presentation of single-layer graphene structure with indicated covalent bonds and π -cloud, and defect in graphene structure and the path of EMW when they hit its surface, reflection, transmission, and absorption from top (left) and side view (right)

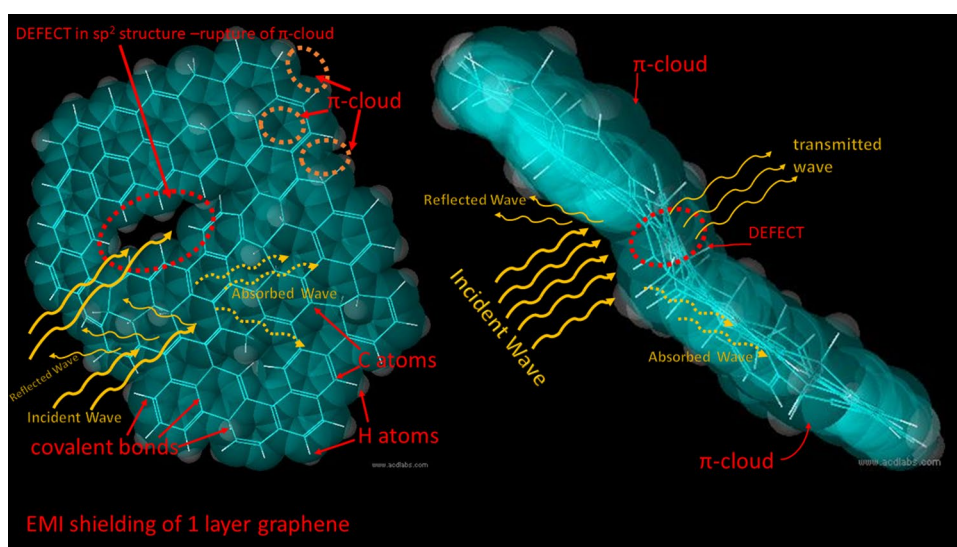
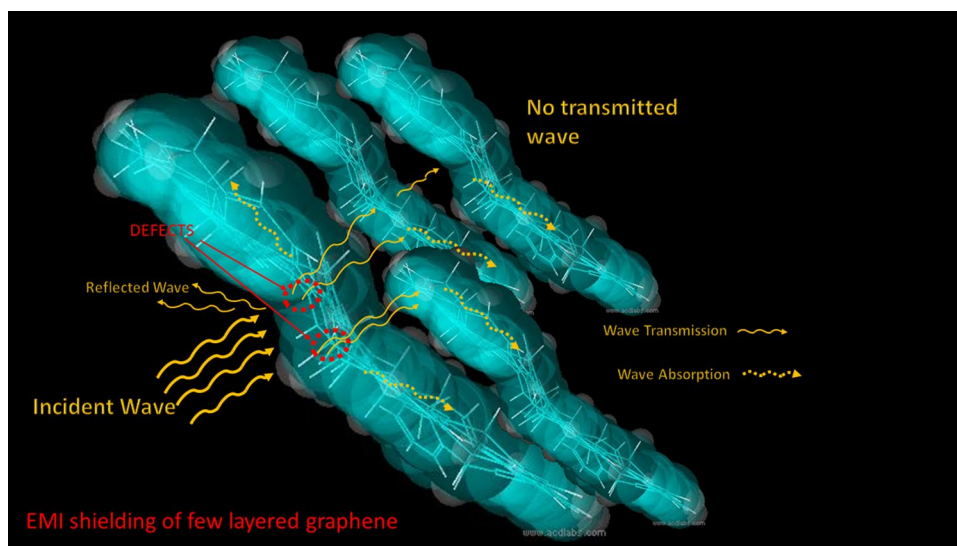


Fig. 6 Schematic presentation of multilayer graphene the path of EMW when they hit its surface, reflection, transmission, and absorption of EMWs



by vacuum deposition, while film thickness was controlled by changing the volume of GO dispersion. Using HI vapor, the chemical reduction was achieved and rLGO and rSGO were produced. The film thickness was from 7.5 to 10 μm . XPS analysis showed that the ratio C/O was 1.56 and 1.79 for SGO and LGO, and it increased to 5.25 and 6.75, respectively, after the reduction. Structural disorder of GO is usually estimated using Raman spectra analysis where the ratio between D and G bands is proportional to defects in graphene structure [61, 93]. In this case, the I_D/I_G peak intensity ratios were 0.93, 0.90, 1.40, and 1.35, corresponding to SGO, LGO, rSGO, and also rLGO films. These values are considered relatively high meaning that in the graphene structure defects are present. XRD showed a 2θ peak of graphite sharply appearing at 26.71° , indicating a d-spacing of 3.34 \AA , while the shift of 2θ peak from 10.39° (SGO) to 26.0° (rSGO) and from 10.7° (LGO) to 26.14° (rLGO) suggest the reduction. With the increase in GO sheets size, drastic enhancement in both electrical ($243 \pm 12 \text{ S cm}^{-1}$) and thermal conductivity ($1390 \pm 65 \text{ W m}^{-1} \text{ K}^{-1}$) was detected. Total EMI shielding effectiveness of both rSGO and rLGO thin films in L and S bands (300 MHz–4 GHz) frequency range with various thicknesses:

- 3 μm shows EMI SET values of ~ 4.5 and 6 dB for rSGO and rLGO,
- 7.5 μm reaches up to ~ 15 dB for rLGO film and ~ 12 dB for rSGO film at 1 GHz,
- two films of 7.5 μm thicknesses together (total thickness $\sim 15 \mu\text{m}$): ~ 20.2 dB (rLGO) and ~ 17 dB (rSGO).

EMI SE value increases with the film thickness. This indicates that not only electrical conductivity but also the thickness of the shielding materials plays a key role in EMI shielding efficiency. For rLGO of thickness $\sim 15 \mu\text{m}$, SE_T , SE_R , and SE_A were measured to be ~ 20.2 , 5.55, and 14.65 dB, respectively. A similar trend was found for rSGO with smaller sheets, where SE_T , SE_R , and SE_A were ~ 16.7 , 5.42, and 11.28 dB, respectively. These results suggest that graphene films have both reflective and absorptive characteristics to electromagnetic radiation; with absorption as the dominant shielding mechanism. But also, these results indicate that sheet size does not play a key factor in the EMI shielding of graphene.

The graphene pellet was produced in the CVD procedure and analyzed as a free-standing film for EMI shielding [94]. The thickness of the film was 50 μm , electrical conductivity was 1136 S/cm, and EMI shielding efficiency was 60 dB.

For graphene paper, EMI SE was between 53 and 55 dB [95]. The material was obtained using five-stage process, from graphite thermal exfoliation at 1150°C , sonication, vacuum filtration, thermal annealing (up to 450°C), and mechanical compression (5 MPa). The conductivity

of 443 S/cm was achieved and reached 1435 S/cm after compression.

In another study, GO flakes in three different sizes (5–8 μm , 20–30 μm , and 40–50 μm) were used to obtain GO free-standing films [96]. The reduction was achieved by thermal treatment at 2600°C , and samples were mechanically compressed at 300 MPa maximal. The highest SE was measured for the film prepared from the largest GO flakes (73.7 dB) and it was noticed that mechanical compression leads to lowering the EMI SE. This phenomenon was explained by pore crashing. Namely, in free-standing graphene films, insulated air pores and graphene walls are present. When the incident EMWs hit the interference between graphene and air pore, one portion of EMW is transmitted while the other is reflected, and multiple reflections and transmissions are repeated infinitely between graphene walls in the lamellar structure of free-standing films. But after compression, the distance between the wall in pores is lowered which leads to destructive interference of EMWs.

One more study investigated free-standing graphene films [97]. Herein, GO was first obtained using chemical exfoliation of graphite using sodium perborate (BH_8NaO_7) and concentrated H_2SO_4 . Vacuum filtration followed by mechanical compression (20 MPa) was used to obtain graphene film. Graphene with low defect and low O content (1.8–2.6 at%) was produced. Very thin free-standing films of 1.6 and 3.2 μm showed astonishing EMI SE of 33 and 68 dB, respectively. This is a record shielding efficiency compared to the sample thickness. The main shielding mechanism was absorption. Figure 7 presents the structure of GO with indicated defects such as wholes and O-functional groups, as well as the interaction with EMWs and absorption.

With the doping of graphene sheets, the EMI SE was largely improved [98]. Herein, researchers selected large graphene sheets, doped them with iodine, and produced free-standing films with a remarkable EMI SE of 52.2 dB, when the sample thickness was only 12.5 μm . Using GO dispersion, free-standing films were obtained by vacuum filtration, and annealed at 1600°C in Ar atmosphere, followed by exposing to I_2 vapor at 200°C to incorporate I atoms in the graphene structure. Apart from EMI shielding efficiently, the material showed astonishing electrical conductivity of $1.05 \times 10^5 \text{ S/cm}$. Also, when graphene was doped with only 1.95 at% of S atoms, produced free-standing films showed the EMI shielding efficiency of 38.6 dB [99], and around 33.2 dB for graphene doped with 5.6 wt% of sulfur [100], and for ultrathin films with nitrogen (7.89 at%) SE was 58.5 dB [101]. This remarkable increase in the EMI SE was explained by the increase in the electron density in the graphene π -cloud, as can be observed in Fig. 8, where S-, N-doped GO was presented. Although heteroatoms increase structural disorder, if they have higher electronegativity or are incorporated into the graphene structure

Fig. 7 GO structure with marked wholes and O-functional groups (left) and interaction with EMWs leading to dipole and charge relaxation, absorption and transmission (right)

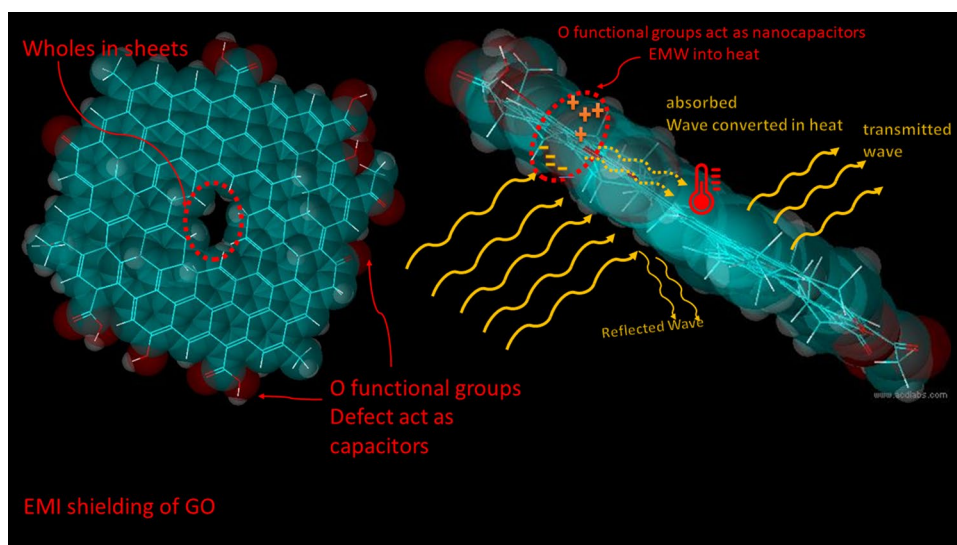
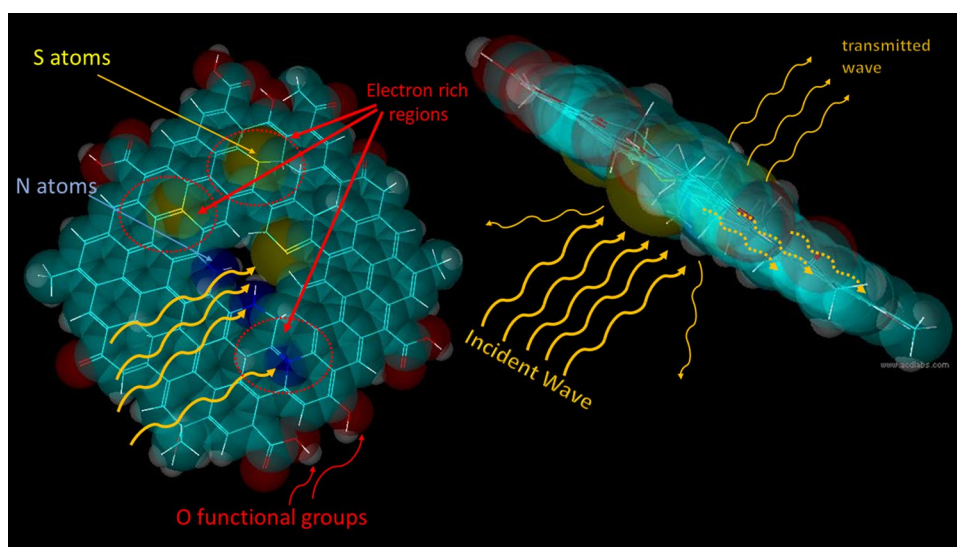


Fig. 8 The structure of heterodoped GO (left) and side view of the same one in the interaction with EMWs (right)



as electron-donating functional groups [102, 103], these atoms lead to an increase in electron density in the graphene π -cloud, improving electrical conductivity as well as EMI SE.

To reduce the processing time and materials need for reduced GO film production, GO dispersion was deposited on the Zn foil which served as a support and as a reducing agent [104]. The EMI SE was between 12.75 and 33.50 dB. Graphene functionalized with polyvinylidene fluoride (PVDF) showed an EMI SE of 20 dB in the X-band (8–12 GHz) [105].

One more free-standing rGO film was produced by thermal reduction of GO film [106]. Here, GO contained 19 at% of O, while after reduction O at% was 13, according to XPS. With a thickness of $93.1 \pm 12.4 \mu\text{m}$, rGO free-standing film showed EMI SE 61.6 dB at 12.4 GHz. A key factor in

the high SE_T is the reduction of graphene and restoration of sp^2 structure, which resulted in electrical conductivity of $1.17 \times 10^4 \text{ S/m}$.

A porous 3D, graphene-based nanomaterial was produced using the CVD approach and porous Cu/Ni foils as a catalyst and template [107]. The walls of the pores were built from 2 to 5 graphene layers. Materials showed extraordinary EMI SE of above 720 dB cm^3/g and SSE_T higher than 45 000 dB cm^2/g . Pores sizes were 60 μm , density 20–33 mg/cm^3 , the porosity of 98.5–99.0%, and surface area was 26 m^2/g , while electrical conductivity was amazing at $1.5 \times 10^5 \text{ S/m}$. XPS analysis showed that the material contained only 1.8 at. % of O, while the rest was C mostly in sp^2 configuration. The surface of the 3D foam was hydrophobic with a 105° of contact angle. Electrical conductivity motivated the researchers to investigate EMI SE in the frequency

range of 8–12 GHz. For these measurements, 3D graphene was filled with polydimethylsiloxane (PDMS) polymer, and materials showed SE from 0.3 to 40 dB, when thicknesses were varied from 1 to 100 mm. The main shielding mechanism for this material was absorption.

Analysis of these papers leads to the following conclusions:

- Graphene is able to absorb EMW;
- The reduced form of graphene oxide is a more efficient shielding material compared to GO;
- The thickness of graphene plays a very important role in EMI shielding, and it increases with the graphene layer number;
- Although defect-free graphene is highly efficient in shielding, better efficiency can be achieved with increased layer number;
- Even graphene oxide films with defective structures that are electrically non-conductive are capable of blocking EMWs;
- Incorporation of electron-rich atoms in graphene sheets leads to N-doping, an increase in electron density, and eventually an improvement of electrical conductivity as well as EMI SE.

2.2 AgNWs composites in EMI shielding

Although graphene has been produced in the electrically conductive form, the procedure for obtaining this type of material can be expensive, the size of graphene could be limited by chamber size (CVD or thermally annealing), while the chemical reduction is often demanding and dangerous (such as the use of heating in H_2 atmosphere), leading to the production of a large amount of residual chemical reagents and solvents. Thus, combining GO with electrically conductive and very thin nanostructures such as silver nanowires is one of the successful strategies to produce new nanocomposite materials efficient for EMWs shielding. Silver nanowires are being used for the fabrication of highly conducting composite materials including thin films, sandwich structures, foams, and fibers due to their high conductivity [108–117]. Nevertheless, AgNWs undergo chemical changes that are accelerated by high humidity and temperature, light, and H_2S , forming acanthite (Ag_2S), oxide (Ag_2O), or chlorargyrite ($AgCl$) layers [118–121]. Ag_2S is a semiconductor with lower electrical conductivity than bulk silver [122], due to the formation of nanoparticles on the AgNWs surface [119]. Thus, to achieve long-term stability, AgNWs must be protected with a layer of material that will block their contact with water and air [123].

EMI SE of AgNWs was studied in different complexes and various efficiencies were measured, from 15 dB as sandwich structure poly(ether sulfone) (PES)-AgNWs-polyethylene

oxide (PEO) [124], 18 dB (3–17 GHz) for AgNWs in epoxy resin with 3-aminopropyltriethoxysilane (APTES) [125], 50 dB (0.5 GHz) for AgNWs with polyaniline (PANI) [126], 70 dB (8–18 GHz) for AgNWs in carbon aerogel [127], around 64 dB for AgNW deposited on textile and covered by PU [128], 56 dB (X-band) for AgNWs deposited on silk with transition metal carbide/carbonitride (MXene) nanosheets [129], 32 dB (X-band) MXene/AgNW-PVA [130], 48 dB for AgNWs coated with $Ti_3C_2T_x$ MXene [131], 50 dB for MXene/AgNW/PU composite foam [132], 30.5 dB for the PET/AgNW/ $Ti_3C_2T_x$ /PVA-PSS film [133], 81 dB for $Ti_3C_2T_x$ MXene-silver nanowire [134], 59 dB for textile immersed in AgNWs/polyvinyl butyral (PVB) mixture [135], 45.9 dB for AgNWs with biodegradable poly(3-hydrobutyrate-co-3-hydroxyvalerate) (PHBV) [136] or 27.6 dB with other biodegradable polymer poly(L-lactic acid) [137], 97.3 for AgNWs with thermoplastic polyurethane (TPU) [138], 27 dB woven Ag-NW 3D networks, 66 dB for AgNWS with acrylamide (AAm) and N-acryloyl-11-aminoundecanoic acid (A-11) aerogel [139], 19.1 dB AgNWs with PEDOT:PSS [140], 48.6 dB for AgNW polyimide composite foams [32].

Graphene oxide due to its mechanical flexibility, a large number of negatively charged functional groups and large surface area, easily creates complex with AgNWs, covering their surface which leads to the preservation of their structure and the electrical properties [141]. Thanks to various synthetic procedures, GO could be obtained in different sizes, oxygen content, and at various prices. Due to these facts, numerous studies investigate the properties of GO–AgNWs composites, while its EMW SE becomes more efficient and shows various advantages that will be discussed in the following part.

2.2.1 Graphene oxide/silver nanowires composites for EM Shielding

One of the first studies investigating graphene-AgNWs-based composite as the shielding material was published in 2015 [34]. Herein, AgNWs were prepared in the form of networks by multistep drop-casting them on quartz substrates. Then, CVD-produced single-layered graphene (SLG) was placed covering only the half of AgNW network. Laser irradiation was applied with a pulse of 248 nm and $\Delta\tau$ of 25 ns, at a repetition rate of 10 Hz. These experiments proved that graphene perfectly protected AgNWs that were beneath the graphene layer. Both the shape and the size of NWs were intact. On the opposite, a severely damaged region of NWs was observed when laser irradiation was directly applied to the AgNWs surface. Herein, laser irradiation induced fragmentations and cutting of AgNWs. Even single-layer graphene created a protective thermal barrier that preserved NWs.

In another study, composites made of the AgNWs with a diameter between 15 and 35 nm, and a length of 15–25 μm and Hummer's method produced GO were studied [33]. Large and small GO flakes were separated by centrifugation. The free-standing, sandwich films were prepared by vacuum deposition onto the porous membrane using the following deposition procedure: GO water dispersion was run through the membrane, then AgNWs were deposited, and GO was deposited one more time. Thus, GO/AgNWs/GO hybrid films were peeled off from a membrane filter. For the chemical reduction of GO in the hybrid film, HI was used. The films were flexible and only 8 μm thick. The C/O ratio was 9 after reduction, while the Raman I_D/I_G ratio (1.4) revealed a large number of defects, and the electrical conductivity was $6.5 \times 10^4 \text{ S m}^{-1}$ when 35 wt% of AgNWs was in the film. Herein, the enhancement in the electrical conductivity and EMI shielding was assigned to the tight contact of the top and bottom graphene layers with the middle AgNW layer. Graphene layers blocked the contacts of AgNW with air and prevent their corrosion and oxidation. EMI SE for the film at the X-band (8.4–12 GHz frequency range) was: 17 dB for rGO, 24 dB with 10 wt% AgNW content, and 38 dB with 35 wt% AgNW loadings. EMI shielding mainly depends on the electrical conductivity of the sample. So, improved EMI shielding was a result of increased conductivity, while the main shielding mechanism was assigned to the absorption of EM.

Later, in 2018, rGO/AgNWs composites were produced and atmospheric pressure plasma jets (APPJs) treatment was applied to increase the electrical conductivity [35]. Herein, AgNWs were produced by the polyol method while graphene was obtained by high shear speed treatment of expanded graphite (eG). Conductive ink was obtained by mixing AgNW and eG in different mass ratios (60:40, 40:60, 30:70, and 20:80). Inks were deposited on glass, textile fabric, and PET followed by APPJ treatments, for up to 15 s. AgNWs were 30–50 nm in diameter and 30–50 μm length, while graphene sheets were composed of 3–15 layers and 10 to 30 μm in lateral size, with low oxygen concentration (4.48 at%) and the O/C ratio of 0.041. Interconnections between AgNWs (30–50 nm) and graphene were accomplished in two ways: direct crossed-wire junctions at the lateral level and over graphene with wires vertically in the next layer. Structural analysis revealed additional disorders and defects due to AgNWs incorporation in graphene sheets and a charge doping effect between the two materials in the film. Graphene acts as a physical barrier and protects AgNWs from both oxygen and moisture due to its gas barrier and superhydrophobic properties, leading to moisture repellence.

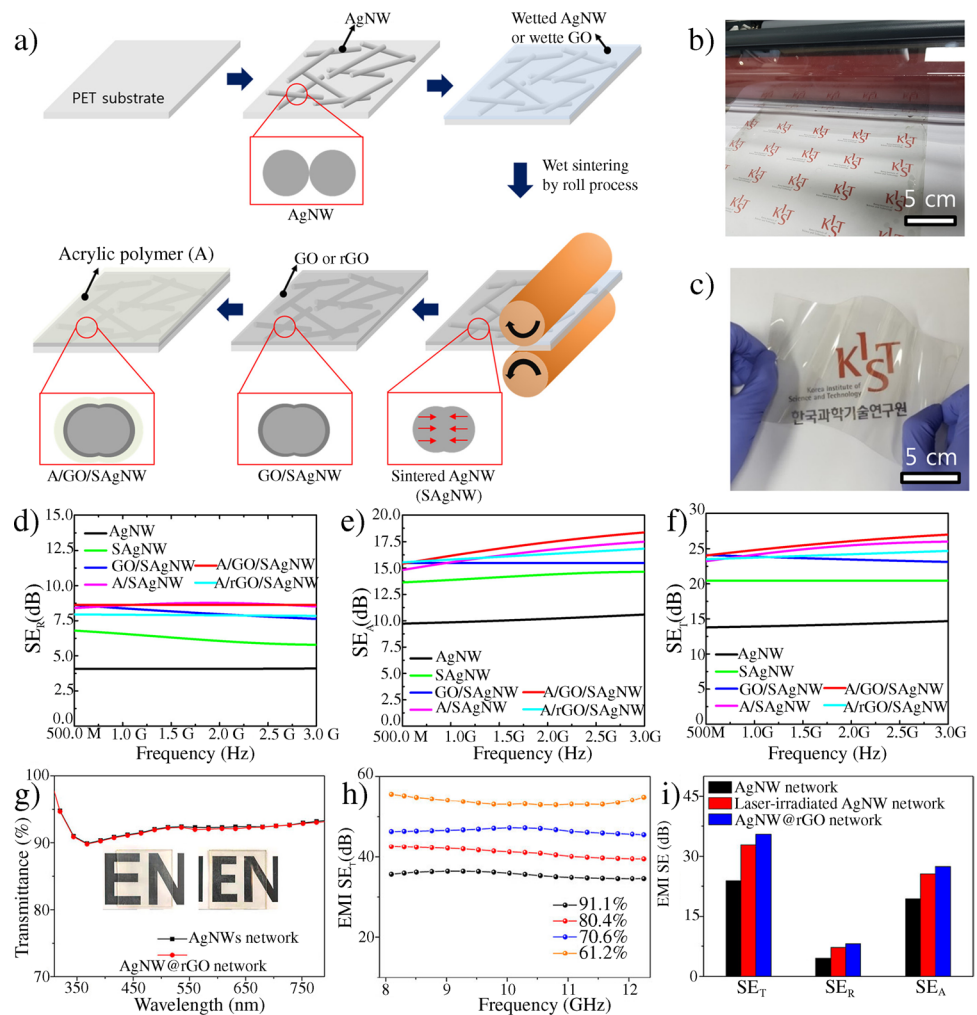
One more transparent EMI shielding film was prepared using AgNWs and GO on a PET substrate [36]. First, AgNWs (35–45 nm in diameter and 5–15 μm in length) were dispersed at a concentration of 0.5 wt% in isopropyl alcohol

(IPA) and wet-coated onto the PET substrate, dried using a hot plate (Fig. 9a). AgNW films were sprayed or coated with water or a water-based GO suspension and after the AgNWs were wet-sintered with a roll-to-roll system at temperatures of 40–140 $^\circ\text{C}$, dried, and reduced with hydrazine vapor. The acrylic microemulsion was spin-coated onto these films and highly transparent material was obtained (Fig. 9b, c). The sheet resistance was reduced from 38.9 to 34.8 Ω/\square at 140 $^\circ\text{C}$. EMI shielding performance was improved compared to pure AgNWs: SE_R values were increased by 2.1 times, from 4.1 to 8.6 dB (at 1 GHz) at the same optical transmittance (90.3%), SE_A value of AgNW increases by approximately 1.5 times from 9.4 to 13.9 dB as compared to that of the pristine AgNWs at the same optical transmittance (90.3%) (Fig. 9d–f). Total EMI SE values were around 20 dB at a frequency of 0.5–3 GHz.

Another GO–AgNWs composite was prepared by simple mixing GO dispersion (1 wt% in water, flake size 40 μm) with AgNWs (1 wt%, ethanol, diameter \sim 37 nm, the length above 10 μm) [37]. Mass ratios varied from 20 to 80 wt%, and free-standing films were produced by drying dispersion in a Teflon mold. Composites were deposited to the cotton textile by immersing in the ink with 80 wt% content of AgNWs. The self-healing performance was investigated by measuring EMI SE, followed by partially breaking and then water spraying onto the damaged region. A high electrical conductivity of $2.9 \times 10^6 \text{ S/m}$ was measured and a relatively low density (2.9 g/cm^3). The EMI SE in the 80 wt% composite films reached 72 dB at 8.2 GHz [37]. The highest electrical conductivity was $2.9 \times 10^6 \text{ S/m}$ in the film with 80 wt% of AgNWs. When the content of AgNWs increases, the number of electrical pathways was enhanced, resulting in reduced electrical resistance and increased film conductivity. EMI shielding mechanism was explained by the multilayered structure. When the EMWs first strike the surface of the composite, some waves were reflected through interactions with free electrons on the surface, while the remaining wave penetrates the composite, and further interactions with free electrons cause a loss of electromagnetic energy. The energy loss phenomenon was repeated at each layer through the thickness of the composite and EMW energy was significantly decreased as it passes through the film. When AgNWs content increased, both the SE_{total} and SE_A were enhanced [37]. This GO–AgNW composite (with 80 wt% of NWs) showed a total EMI SE of 92 dB, 18 μm thick, and highly flexible. On cotton, a total EMI SE was 32 dB while the textile was highly flexible, had mechanical stability during 1000 bending cycles, self-healing properties, and high potential to apply in EMI cloth for wearable devices, aerospace, and military applications.

Composite with Hummer's produced GO flakes and polyol-synthesized AgNWs was partially reduced with vitamin C, freeze-dried, and backfilled with PDMS [39].

Fig. 9 Schematic presentation of composite production (a), photographs of resulting materials (b and c), EMI SE_R (d), EMI SE_A (e), EMI SE_T (f) components for different stages of material production, reprinted with permission from highly bendable and durable transparent electromagnetic interference shielding film prepared by wet sintering of silver nanowires, by Dong Gyu Kime et al., ACS Appl. Mater. Interfaces 2018, 10, 29,730–29,740 [36]. Copyright 2023 American Chemical Society. Transmission spectra (g), EMI SE_T of composites with different AgNWs and GO loadings (h), values of EMI SE_{Tr} and EMI SE_A (i). Reprinted with permission from Reduced Graphene Oxide Conformally Wrapped Silver Nanowire Networks for Flexible Transparent Heating and Electromagnetic Interference Shielding by Yang et al. ACS Nano 2020, 14, 8754–8765 [44]. Copyright 2023 American Chemical Society



Electrical conductivity was 12.1 S/cm, EMI SE in X-band was enhanced with the increase in AgNWs and reaches the highest value of 34.1 dB at 0.43 wt% rGOs and 0.33 wt% AgNWs loadings. Thanks to the segregated structure of the composite, the incident EMWs easily penetrate the composite and were attenuated thanks to the synergistic behavior of two facts, outstanding electrical conductivity and porous inner structure.

More recently, GO–AgNW composite was produced by electrochemical deposition [44]. Herein, AgNWs were produced directly at the PDMS, a flexible substrate using electrospinning and subsequent electroless deposition. First, a precursor for nanoseeds for AgNW production was produced by electrospinning of PVB and SnCl_2 in a nonpolar solvent, n-butanol. Then, the AgNW network was formed from Tollen's reaction when Ag was deposited by electroless depositing on the templates. When AgNW was obtained, GO flakes were deposited using electrodeposition. Electrolyte was GO water dispersion (0.25 mg/ml), while the electrodes were iridium sheet and AgNW network. During the electrochemical reaction, GO was deposited on AgNWs

supported and reduced with a nanosecond pulse laser. Structural order was improved, as Raman ratio I_D/I_G was lowered from 1.1 to 0.7, while XRD showed that an average grain size was increased from 25 to 45 nm, for the GO–AgNW and rGO–AgNW samples. With a transmittance of an amazing 91.1%, the rGO–AgNWs had a high SE_T of 35.5 dB and lowered for only 10% after 1000 cycles of stretching and releasing (Fig. 9g–i). These materials showed extraordinary durability, transmittance, and EMI SE.

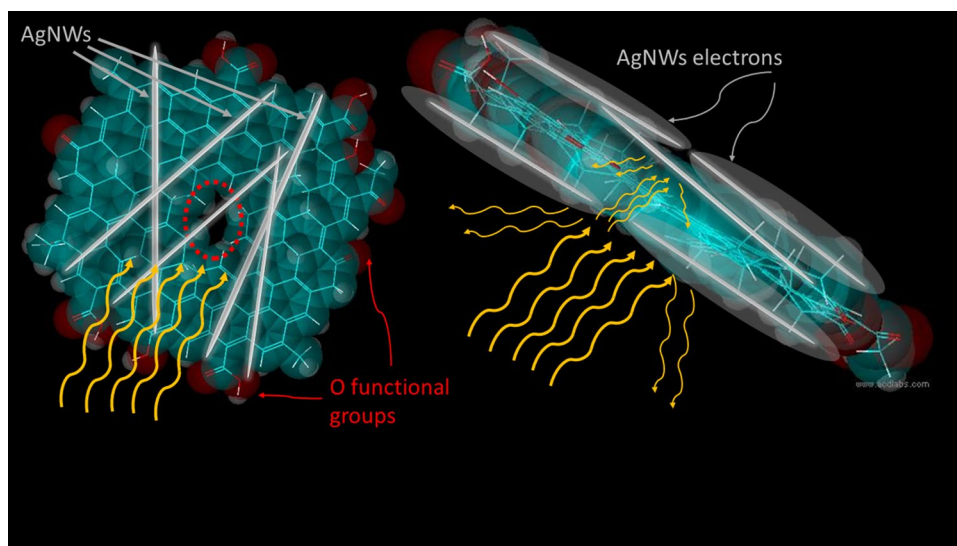
Another similar composite, with GO and AgNWs to block EMI, was produced by Jia et al. [45]. Different from other studies, herein GO has not been subjected to any chemical nor physical approach for the reduction of O-containing functional groups, while the size of flakes was between 500 nm and 2 μm . AgNWs were 40 nm in diameter while their length varied from 20 to 45 μm . A free-standing GO–AgNWs composite with a multilayered structure and low thickness was produced using vacuum filtration and a layer-by-layer self-assembly approach. First, layers of GO were deposited, by pouring 6 mL of GO dispersion followed by 8 mL of AgNWs. Obtained multilayer samples were

exposed to the pressure of 20 MPa for 5 min. GO flakes were negatively (-47.4 mV) and AgNWs were positively charged ($+16.2$ mV), thus electrostatic interaction was built. GO flakes were wrinkled due to the capillary force between the sheets and nanowires during water evaporation. Composite without compression showed electrical conductivity of 56.88 S cm^{-1} , while the multilayered structure varied from 1144.3 to 2255.8 S cm^{-1} . EMI SE in the range of 18–26 GHz frequency (K band) was 60.7 dB for AgNWs, and for the multilayer GO/Ag-xL was 55.16 dB. The density-specific shielding effectiveness was 25.55 , while for GO/Ag-3L was 56.22 dB cm^3 g^{-1} . They found that SE_T was a positive connection between conductivity and it was following Simon's formula. For multilayer samples, the main EM shielding component is absorption and it is related to the ability of EM waves to enter the material. By comparing absorption and reflection, most of the reflected waves occur in the layer of AgNWs with the highest electrical conductivity. Authors suggested that EM shielding is a result of multiple reflections and multiple absorptions. When the EM waves hit the GO layer which is not conductive, a weak reflection occurs, and a large fraction of the EM wave enters the material and travels until it reaches the highly conductive layer of AgNWs, as presented in Fig. 10a. Then, waves are reflected while the rest of the wave is reduced by hitting the next GO layer, as other reflections in from AgNWs, as it is presented in Fig. 10b and c. In the case of multiple absorptions, when EM waves hit the GO it has been absorbed in defects sites and O-functional groups, and it is acting as nano-capacitor. Defect leads to inhomogeneity in electron cloud density as well as charges, causing the dipole and charge polarization relaxation. Thus, EMW are converted into heat, while in AgNWs layer charge carriers lead to conducting, hopping, and tunneling producing the surface current. EMWs could

be covered in Joule heat or reflected from the AgNWs layer to the GO phase where multiple absorption leads to EMW blocking.

Aerogel based on GO and AgNW was produced and studied as an EMI shielding material [142]. Simple mixing of GO water dispersion with AgNWs, followed by the addition of reducing agent ascorbic acid and ambient pressure drying, was proposed. Authors reported that GO sheets were $5\text{--}8$ μm with folded wrinkles, while AgNWs were 60 nm in diameter and a length from 20 to 30 μm . An interesting morphology was observed: AgNWs were interconnected and attached to the wrinkled GO layers. This aerogel had an abundant porous structure, with pore size from a few microns to several hundred microns and homogenous distribution of both AgNWs and rGO in the hybrid material. The reduction leads to a remarkable increase in the C/O atom ratio from 2.6 to 6.6 . Raman analysis proved that defects of graphene sheets created by oxygen-containing groups were partially repaired in aerogel due to a lowering in I_D/I_G ratio from 2.08 to 1.59 . In this composite, AgNWs were tightly bonded to the surface of rGO sheets and become a bridge which was connecting sheets and it is associated with the resistance for deformation. For rGO, EMI SE was 17.1 dB, while for aerogel with increased AgNWs content, the SE_R component remained low, but SE_A was increasing. The highest EMI SE was 45.2 dB. When incident waves enter the shielding materials, the interaction between the free carriers (electrons and holes) with waves resulting in the formation of induced currents caused dissipation of the EWs energy. The parallel process is occurring as the movement of induced currents generates an induced electromagnetic field in the materials to further decay incident waves. With larger AgNWs content in the material, electrical conductivity is higher as well and more free carriers are present in the material which are

Fig. 10 Schematic presentation of the structure of GO–AgNWs, side view of composite and interaction with EMW with composites, and interaction of EMWs with multilayer composite



moving and consuming EWs. Furthermore, AgNWs created links among graphene sheets making the electron transport channels that accelerate the EW consumption. The dissipation of EMW is connected with induced currents and an induced EM field. Both currents and fields interact with incident waves and induce the transformation of the wave's energy into heat energy. A porous, 3D network structure redistributes the EM field and improved wave attenuation. Thus, an appropriate combination of material and its inner structure and porosity, hide the impressive strategy for EMW attenuation and shielding.

By combining GO with good mechanical but poor electrical properties with AgNWs with excellent conductivity but limited elasticity, strength, and chemical stability, improved complexes are simply obtained and showed astonishing shielding properties, with SE from 20 dB at a frequency of 0.5–3 GHz [36], 31 db [143], 34.1 dB [39], 35.5 dB [44], 38 dB (8.4–12 GHz frequency range) [33], 45.2 dB [142], 60.7 [45], to 72 dB at 8.2 GHz [37], 76.6 dB [144]. Composites were prepared in the form of free-standing layers, at various supports including cotton, glass, or PET as well as an aerogel. Several shielding mechanisms were proposed:

- Reflection from conductive AgNWs layers to the GO layer that is absorb the part of reflected waves,
- Multiple absorption and multiple reflections inside the layered structure of GO–AgNWs,
- In defect sites and O-functional groups, and it is acting as nano-capacitor and causing the dipole and charge polarization relaxation,
- Incident EMWs induced currents and an induced EM field lead to the transformation of the wave's energy into heat energy.

2.2.2 Graphene oxide/silver nanowires–polymers composites for EM shielding

Apart from pure graphene, and graphene with AgNWs, various composites with polymers were produced with the aim to increase the durability, mechanical strength, elasticity, and improve transparency or EMI SE by combining these composites with conductive polymers [39, 145–151]. Electrical non-conductive polymers are fully transparent to EMW due to a lack of electric and magnetic dipoles as well as electrical conductivity [152]. For instance, polycarbonate with electrical conductivity of 10^{-12} – 10^{-14} S/m shows SE_T of 0 dB [153]. By combining PC with magnetic or metallic fillers, this polymer could be converted into efficient EMI shielding material [154–157]. Conductive polymers such as polypyrrole, polyaniline, and polythiophene due to their high electrical conductivity and good dielectric properties, are highly efficient EMI shielding material, as well as their composites [158–161]. This study is focused on the effects of graphene

which is why the composites with these polymers which possess itself EMI SE will not be discussed further.

In Table 2, the EMI SE of various graphene-based composites and their thickness and transparency were presented. These results showed that graphene samples could have both high EMI SE and transparency, as presented in Table 2.

When graphene was functionalized with both graphene quantum dots (GQDs) and silver nanoparticles and incorporated in polyvinylidene fluoride (PVDF) by solution blending, a high EMI SE was observed [38]. Only 2 wt% of graphene composite was used to produce a modified polymer with a total EMI SE (SE_T) of 43 dB at 8 GHz while a reflection contribution of 50.3% [38].

Composite based on polyurethane and GO/AgNW was investigated too [40]. The diameters and lengths of the AgNWs in the IPA suspension (0.5 wt%) were 20–25 nm and 25–30 μ m, respectively. A hydrophobic silane-functionalized graphene–urethane rubber (HS/G–UR) with AgNWs was overcoated on PET support. In this way, a durable, bendable material was produced with SE_T of 18.9 dB.

GO–AgNW composite was prepared during the process of AgNW synthesis [41]. Herein, during AgNW polyol-synthesis, GO dispersion in EG (1 mg/ml) was added to the reaction mixture. During this stage, GO was reduced and formed rGO/AgNWs complex. This solution was coated onto a PET substrate with coating rods. Silver grids were printed on the second PET. Two supports were put together face-to-face on a hot press. Raman spectroscopy proved the chemical reduction of GO, while electrical resistivity was $1.6 \Omega/\square$, transparency was 74.4%, and EMI SE was 42.9 dB at 1.8 GHz.

Ma et al. fabricated a polymethyl methacrylate (PMMA)/graphene/metal mesh hybrid film with the EMI SE of up to 28.9 dB at 12–18 GHz while the sheet resistance of graphene was significantly suppressed from 813.27 to 5.53 Ω/sq when the light transmittance was 91% [42].

The liquid phase stripping method was used for graphene synthesis afterward individual dispersions of G and AgNWs in ethanol were mixed [43]. To produce shielding layers, on the glass substrate, different materials were spin-coated, first PEDOT:PSS, followed by AgNWs, and the graphene solution. Using water, PEDOT:PSS was dissolved and detached from the glass support. TEM analysis showed wrinkled graphene flakes. It was assumed that these wrinkles are responsible for bending resistivity and flexibility. Very high light transmittance was measured for one layer (78.4%). For a film with a thickness of 30 μ m, EMI SE was 40.1 dB and 47.0% transmittance, while for the most transmitting film, EMI SE was 28 dB.

Over the years, several approaches for obtaining composites based on graphene/GO and AgNWs have been developed:

Table 2 EMI SE, sample thickness, and transparency of the sample

Material	SE _T (dB)	Thickness	Transparency (%)
CVD graphene [91]	2.27	0.4 nm	98.3
PEI/RGO [162]	6.36	20 nm	62
Graphene/PMMA [163]	48%	800 nm	97.8
Graphene/PET [92]	19.14	4 nm graphene	80.5
Metal mesh/graphene [164]	14.1	–	97.3
graphene/metallic mesh/transparent dielectric	67.9	–	85
Graphene/metal network [42]	20.67	320 μm	94
Acrylic polymer-coated/rGO/AgNWs [92]	24	–	85
Ni mesh/GO [165]	12.1	20 nm	83
PVA GNR ^a —Fe ₃ O ₄ [166]	16.36	–	79.8
Ti ₃ C ₂ T _x MXene-PU-AgNWs [167]	27.8	–	86
Epoxy/carbon nanotube sandwich [168]	23.4	6 mm	0
Graphene mesh [169]	3.86	3–5	95
PDMS/AgNWs/TCP [169]	39.1	–	86.8
PET/AgNWs/rGO [170]	33.6	–	82

^aGNR-graphene nanoribbons

^bTCP-transparent cellulose paper

1. AgNWs colloid deposited on support followed by on-top synthesis of graphene using CVD [34],
2. AgNWs colloid and GO dispersion mixed in different volume/mass ratios [33, 35, 37],
3. wet-coating of AgNWs on PET support followed by a coating of GO dispersion [36],
4. aerogel of GO flakes and polyol-synthesized AgNWs backfilled with PDMS [39],
5. synthesis of AgNWs on supports by electroless depositing techniques followed by GO electrodeposition [44],
6. vacuum filtration to achieve layer-by-layer self-assembly of GO and AgNWs [45],
7. aerogel was obtained by GO water dispersion mixing with AgNWs followed by reduction [142],
8. in situ synthesis of AgNWs on GO flakes by hydrothermal route [144].

Due to simplicity, the quick establishing of the interactions between GO and AgNWs, the possibility to produce the composite at a large scale, processability, and the ease of control of the content of each component of the composite, the method listed under 2 is mostly used in AgNWs-GO preparation.

Thanks to excellent flexibility, transparency, processability, and a high EMI SE, these films showed great promise in various applications, from instrument protection, car, and other vehicles industry, to the application textile industry.

3 Conclusion

Graphene and its composites are being increasingly studied as EMI SE materials. With the development of synthetic methods and possibilities to modulate graphene structure, EMI shielding efficiency is getting higher. The mass-scale production of graphene requires it to be both cost-effective and ecologically friendly. Most of the recent studies performed in recent times considering graphene for shielding applications involve the production of graphene with either the Hummers method or the CVD method. It seems that the electrochemical exfoliation of graphite for graphene production has great potential and many advantages for example due to avoidance of chemical use, mild conditions, simplicity as well as the potential to be transferred to a large scale. Various possibilities to doped graphene structure from heteroatoms to functionalization with electron-donating functional groups lead to improvements in the electrical conductivity of this material as well as its EMI SE. In the future, the development of new, green approaches for graphene doping, such as hydrothermal approach, microwave or laser-induced doping, or gamma irradiation could highly improve graphene EMI shielding behavior. Due to their chemical properties, AgNWs create complex easily with GO and highly improve electrical conductivity and EMI SE. However, they are not stable in the environments. Combining graphene or GO with AgNWs with different polymers is a promising strategy to produce commercial proactive cover against EMWs that are

efficient shielding materials, transparent, durable, stable, lightweight, and thin.

Acknowledgements This work was supported by the EU, Horizon Europe program. Coordination and Support Action, project Twinning for new graphene-based composites in electromagnetic interference shielding—GrInShield (No. 101079151), and by the Ministry of Science, Technological Development and Innovation of the Republic of Serbia [Grant Number 451-03-68/2023-14/200017]. Also, the authors thank Ph.D. student A. Misovic for preparing figure 1.

Author contributions SJ wrote the main manuscript text, MH prepared sect. 2.2.2, DK worked on sect. 2.1, MY prepared sect. 2, introduction part, and KH worked on sect. 2., sect. 2.2.2. All authors reviewed the manuscript.

Declarations

Conflict of interest The authors declare no competing interests.

Open Access This article is licensed under a Creative Commons Attribution 4.0 International License, which permits use, sharing, adaptation, distribution and reproduction in any medium or format, as long as you give appropriate credit to the original author(s) and the source, provide a link to the Creative Commons licence, and indicate if changes were made. The images or other third party material in this article are included in the article's Creative Commons licence, unless indicated otherwise in a credit line to the material. If material is not included in the article's Creative Commons licence and your intended use is not permitted by statutory regulation or exceeds the permitted use, you will need to obtain permission directly from the copyright holder. To view a copy of this licence, visit <http://creativecommons.org/licenses/by/4.0/>.

References

1. Tiikkaja M, Aro AL, Alanko T, Lindholm H, Sistonen H, Hartikainen JEK, Toivonen L, Juutilainen J, Hietanen M (2012) Electromagnetic interference with cardiac pacemakers and implantable cardioverter-defibrillators from low-frequency electromagnetic fields in vivo. *EP Eur*. <https://doi.org/10.1093/europs/ace/eus345>
2. Upadhyay S, Upadhyay A, Salehi W, Gupta G (2021) The medical aspects of EMI effect on patients implanted with pacemakers. *Mater Today*. <https://doi.org/10.1016/j.matpr.2021.01.826>
3. Gordon JS, Maynes EJ, O'Malley TJ, Pavri BB, Tchanchaleishvili V (2021) Electromagnetic interference between implantable cardiac devices and continuous-flow left ventricular assist devices: a review. *J Interv Card Electrophysiol*. <https://doi.org/10.1007/s10840-020-00930-8>
4. Carles C, Esquirol Y, Turuban M, Piel C, Migault L, Pouchieu C, Bouvier G, Fabbro-Peray P, Lebailly P, Baldi I (2020) Residential proximity to power lines and risk of brain tumor in the general population. *Environ Res*. <https://doi.org/10.1016/j.envres.2020.109473>
5. Zheng Y, Cheng J, Dong L, Ma X, Kong Q (2019) Effects of exposure to extremely low frequency electromagnetic fields on hippocampal long-term potentiation in hippocampal CA1 region. *Biochem Biophys Res Commun*. <https://doi.org/10.1016/j.bbrc.2019.07.085>
6. Hosseinabadi MB, Khanjani N, Ebrahimi MH, Haji B, Abdolshahfar M (2019) The effect of chronic exposure to extremely low-frequency electromagnetic fields on sleep quality, stress, depression and anxiety. *Electromagn Biol Med*. <https://doi.org/10.1080/15368378.2018.1545665>
7. Gunnarsson LG, Bodin L (2019) Occupational exposures and neurodegenerative diseases—a systematic literature review and meta-analyses. *Int J Environ Res Public Health*. <https://doi.org/10.3390/ijerph16030337>
8. Klimek A, Rogalska J (2021) Extremely low-frequency magnetic field as a stress factor—really detrimental?—Insight into literature from the last decade. *Brain Sci*. <https://doi.org/10.3390/brainsci11020174>
9. Jalilian H, Guxens M, Heikkinen S, Pukkala E, Huss A, Eshagh Hossaini SK, Kjærheim K, Vermeulen R (2022) Malignant lymphoma and occupational exposure to extremely low frequency magnetic fields and electrical shocks: a nested case-control study in a cohort of four Nordic countries. *Occup Environ Med*. <https://doi.org/10.1136/oemed-2021-108120>
10. Toutou Y, Selmaoui B (2012) The effects of extremely low-frequency magnetic fields on melatonin and cortisol, two marker rhythms of the circadian system. *Dialogues Clin Neurosci*. <https://doi.org/10.31887/DCNS.2012.14.4/ytoutou>
11. Toutou Y, Coste O, Dispersyn G, Pain L (2010) Disruption of the circadian system by environmental factors: effects of hypoxia, magnetic fields and general anesthetics agents. *Adv Drug Deliv Rev*. <https://doi.org/10.1016/j.addr.2010.06.005>
12. Toutou Y, Selmaoui B, Lambrozo J (2022) Assessment of cortisol secretory pattern in workers chronically exposed to ELF-EMF generated by high voltage transmission lines and substations. *Environ Int*. <https://doi.org/10.1016/j.envint.2022.107103>
13. Toutou Y, Lambrozo J, Mauvieux B, Riedel M (2020) Evaluation in humans of ELF-EMF exposure on chromogranin A, a marker of neuroendocrine tumors and stress. *Chronobiol Int*. <https://doi.org/10.1080/07420528.2019.1683857>
14. Quesnel-Galván LR, Torres-Durán PV, Elías-Viñas D, Verdugo-Díaz L (2021) Effect of extremely low frequency magnetic fields on oxidative balance in rat brains subjected to an experimental model of chronic unpredictable mild stress. *BMC Neurosci*. <https://doi.org/10.1186/s12868-021-00656-x>
15. Maruthi N, Faisal M, Raghavendra N (2021) Conducting polymer based composites as efficient EMI shielding materials: a comprehensive review and future prospects. *Synth Met*. <https://doi.org/10.1016/j.synthmet.2020.116664>
16. Kruželák J, Kvasničáková A, Hložeková K, Hudec I (2021) Progress in polymers and polymer composites used as efficient materials for EMI shielding. *Nanoscale Adv*. <https://doi.org/10.1039/d0na00760a>
17. Wang L, Ma Z, Zhang Y, Chen L, Cao D, Gu J (2021) Polymer-based EMI shielding composites with 3D conductive networks: a mini-review. *SusMat*. <https://doi.org/10.1002/sus2.21>
18. Guo Y, Qiu H, Ruan K, Wang S, Zhang Y, Gu J (2022) Flexible and insulating silicone rubber composites with sandwich structure for thermal management and electromagnetic interference shielding. *Compos Sci Technol*. <https://doi.org/10.1016/j.compscitech.2021.109253>
19. Yang Y, Chen Y, Wang B, Zhou Y, Chai X, Yan X, Han W, Liu C, Lin P, Xia Y, Zhang H, Liao X (2022) Gradient structure silicone rubber composites for selective electromagnetic interference shielding enhancement and low reflection. *Compos Sci Technol*. <https://doi.org/10.1016/j.compscitech.2022.109688>
20. Lee SM, Kim JH, Ahn JH (2015) Graphene as a flexible electronic material: mechanical limitations by defect formation and efforts to overcome. *Mater Today*. <https://doi.org/10.1016/j.mat-tod.2015.01.017>
21. Novoselov KS, Geim AK, Morozov SV, Jiang D, Zhang Y, Dubonos SV, Grigorieva IV, Firsov AA (2004) Electric field effect in atomically thin carbon films. *Science* 306:666–669. <https://doi.org/10.1126/science.1102896>

22. Xia Y, Gao W, Gao C (2022) A review on graphene-based electromagnetic functional materials: electromagnetic wave shielding and absorption. *Adv Funct Mater*. <https://doi.org/10.1002/adfm.202204591>
23. Naghdi S, Jaleh B, Eslampanah M, Moradi A, Abdollahi M, Einali N, Rhee KY (2022) Graphene family, and their hybrid structures for electromagnetic interference shielding applications: recent trends and prospects. *J Alloys Compd*. <https://doi.org/10.1016/j.jallcom.2021.163176>
24. Li JS, Huang H, Zhou YJ, Zhang CY, Li ZT (2017) Research progress of graphene-based microwave absorbing materials in the last decade. *J Mater Res*. <https://doi.org/10.1557/jmr.2017.80>
25. Raagulan K, Braveenth R, Kim BM, Lim KJ, Lee SB, Kim M, Chai KY (2020) An effective utilization of MXene and its effect on electromagnetic interference shielding: flexible, free-standing and thermally conductive composite from MXene–PAT–poly (p-aminophenol)–polyaniline co-polymer. *RSC Adv*. <https://doi.org/10.1039/C9RA09522E>
26. Jaroszewski M, Thomas S, Rane AV (2018) Advanced materials for electromagnetic shielding: fundamentals, properties, and applications. Wiley, Hoboken
27. Shukla V (2019) Review of electromagnetic interference shielding materials fabricated by iron ingredients. *Nanoscale Adv*. <https://doi.org/10.1039/C9NA00108E>
28. Iqbal A, Kwon J, Kim MK, Koo CM (2021) MXenes for electromagnetic interference shielding: experimental and theoretical perspectives. *Mater Today Adv*. <https://doi.org/10.1016/j.mtadv.2020.100124>
29. Gaoui B, Hadjadj A, Kious M (2017) Novel multilayer arrangement of conductive layers traps the electromagnetic interferences by multiple internal reflections at high frequency in the far field. *J Mater Sci Mater Electron*. <https://doi.org/10.1007/s10854-016-6006-z>
30. Shen B, Zhai W, Zheng W (2014) Ultrathin flexible graphene film: an excellent thermal conducting material with efficient emi shielding. *Ind Eng Chem Res*. <https://doi.org/10.1002/adfm.201400079>
31. Kumar P, Shahzad F, Yu S, Hong SM, Kim YH, Koo CM (2015) Large-area reduced graphene oxide thin film with excellent thermal conductivity and electromagnetic interference shielding effectiveness. *Carbon*. <https://doi.org/10.1016/j.carbon.2015.07.032>
32. Lee TW, Lee SE, Jeong YG (2016) Highly effective electromagnetic interference shielding materials based on silver nanowire/cellulose papers. *ACS Appl Mater Interfaces*. <https://doi.org/10.1021/acsami.6b02218>
33. Kumar P, Shahzad F, Hong SM, Koo CM (2016) A flexible sandwich graphene/silver nanowires/graphene thin film for high-performance electromagnetic interference shielding. *RSC Adv*. <https://doi.org/10.1039/C6RA18652A>
34. Das SR, Nian Q, Saei M, Jin S, Back D, Kumar P, Janes DB, Alam MA, Cheng GJ (2015) Single-layer graphene as a barrier layer for intense UV laser-induced damages for silver nanowire network. *ACS Nano*. <https://doi.org/10.1021/acs.nano.5b04628>
35. Alotaibi F, Tung TT, Nine MJ, Coghlan CJ, Losic D (2018) Silver nanowires with pristine graphene oxidation barriers for stable and high performance transparent conductive films. *ACS Appl Nano Mater*. <https://doi.org/10.1021/acsanm.8b00255>
36. Kim DG, Choi JH, Choi DK, Kim SW (2018) Highly bendable and durable transparent electromagnetic interference shielding film prepared by wet sintering of silver nanowires. *ACS Appl Mater Interfaces*. <https://doi.org/10.1021/acsami.8b07054>
37. Sim HJ, Lee DW, Kim H, Jang Y, Spinks GM, Gambhir S, Officer DL, Wallace GG, Kim SJ (2019) Self-healing graphene oxide-based composite for electromagnetic interference shielding. *Carbon*. <https://doi.org/10.1016/j.carbon.2019.08.073>
38. Lakshmi N, Tambe PJCI (2017) EMI shielding effectiveness of graphene decorated with graphene quantum dots and silver nanoparticles reinforced PVDF nanocomposites. *Compos Interfaces*. <https://doi.org/10.1080/09276440.2017.1302202>
39. Li Y, Li C, Zhao S, Cui J, Zhang G, Gao A, Yan Y (2019) Facile fabrication of highly conductive and robust three-dimensional graphene/silver nanowires bicontinuous skeletons for electromagnetic interference shielding silicone rubber nanocomposites. *Compos Part A Appl Sci*. <https://doi.org/10.1016/j.compositesa.2019.01.025>
40. Choi JH, Lee KY, Kim SW (2019) Ultra-bendable and durable graphene–urethane composite/silver nanowire film for flexible transparent electrodes and electromagnetic-interference shielding. *Compos B Eng*. <https://doi.org/10.1016/j.compositesb.2019.107406>
41. Huang CC, Gupta S, Lo CY, Tai NH (2019) Highly transparent and excellent electromagnetic interference shielding hybrid films composed of silver-grid/(silver nanowires and reduced graphene oxide). *Mater Lett*. <https://doi.org/10.1016/j.matlet.2019.06.058>
42. Ma L, Lu Z, Tan J, Liu J, Ding X, Black N, Li T, Gallop J, Hao L (2017) Transparent conducting graphene hybrid films to improve electromagnetic interference (EMI) shielding performance of graphene. *ACS Appl Mater Interfaces*. <https://doi.org/10.1021/acsami.7b09372>
43. Zhang N, Wang Z, Song R, Wang Q, Chen H, Zhang B, Lv H, Wu Z, He D (2019) Flexible and transparent graphene/silver-nanowires composite film for high electromagnetic interference shielding effectiveness. *Sci Bull*. <https://doi.org/10.1016/j.scib.2019.03.028>
44. Yang Y, Chen S, Li W, Li P, Ma J, Li B, Zhao X, Ju Z, Chang H, Xiao L, Xu H, Liu Y (2020) Reduced graphene oxide conformally wrapped silver nanowire networks for flexible transparent heating and electromagnetic interference shielding. *ACS Nano*. <https://doi.org/10.1021/acs.nano.0c03337>
45. Jia H, Yang X, Kong QQ, Xie LJ, Guo QG, Song G, Liang LL, Chen JP, Li Y, Chen CM (2021) Free-standing, anti-corrosion, super flexible graphene oxide/silver nanowire thin films for ultra-wideband electromagnetic interference shielding. *J Mater Chem*. <https://doi.org/10.1039/D0TA09246K>
46. Prekodravac JR, Kević DP, Colmenares JC, Giannakoudakis DA, Jovanović SP (2021) A comprehensive review on selected graphene synthesis methods: from electrochemical exfoliation through rapid thermal annealing towards biomass pyrolysis. *J Mater Chem*. <https://doi.org/10.1039/D1TC01316E>
47. Yy W, Ni Zh, Yu T, Shen ZX, Wang Hm WuYh, Chen W, Shen Wee AT (2008) Raman studies of monolayer graphene: the substrate effect. *J Phys Chem C*. <https://doi.org/10.1021/jp8008404>
48. Ganguly A, Sharma S, Papakonstantinou P, Hamilton J (2011) Probing the thermal deoxygenation of graphene oxide using high-resolution in situ X-ray-based spectroscopies. *J Phys Chem C*. <https://doi.org/10.1021/jp203741y>
49. Huang HH, De Silva KKH, Kumara GRA, Yoshimura M (2018) Structural evolution of hydrothermally derived reduced graphene oxide. *Sci Rep*. <https://doi.org/10.1038/s41598-018-25194-1>
50. Emiru TF, Ayele DW (2017) Controlled synthesis, characterization and reduction of graphene oxide: a convenient method for large scale production. *Egypt J Basic Appl Sci*. <https://doi.org/10.1016/j.ejbas.2016.11.002>
51. Claramunt S, Varea A, López-Díaz D, Velázquez MM, Cornet A, Círcera A (2015) The importance of interbands on the interpretation of the raman spectrum of graphene oxide. *J Phys Chem C*. <https://doi.org/10.1021/acs.jpcc.5b01590>
52. Wazir AH, Kundi IW (2016) Synthesis of graphene nano sheets by the rapid reduction of electrochemically exfoliated graphene oxide induced by microwaves. *J Chem Soc Pak* 38:11–16

53. Gengler RYN, Badali DS, Zhang D, Dimos K, Spyrou K, Gournis D, Miller JRD (2013) Revealing the ultrafast process behind the photoreduction of graphene oxide. *Natur Commun.* <https://doi.org/10.1038/ncomms3560>
54. Sadhukhan S, Ghosh TK, Rana D, Roy I, Bhattacharyya A, Sarkar G, Chakraborty M, Chattopadhyay D (2016) Studies on synthesis of reduced graphene oxide (RGO) via green route and its electrical property. *Mater Res Bull.* <https://doi.org/10.1016/j.materresbull.2016.02.039>
55. Cai W, Piner RD, Stadermann FJ, Park S, Shaibat MA, Ishii Y, Yang D, Velamakanni A, An MS, An J, Chen D, Ruoff RS (2008) Synthesis and solid-state NMR structural characterization of ^{13}C -labeled graphite oxide. *Science.* <https://doi.org/10.1126/science.1162369>
56. Mišović A, Bogdanović DB, Kepić D, Pavlović V, Huskić M, Hasheminejad N, Vuye C, Zorić N, Jovanović S (2022) Properties of free-standing graphene oxide/silver nanowires films and effects of chemical reduction and gamma irradiation. *Synth Met.* <https://doi.org/10.1016/j.synthmet.2021.116980>
57. Ferrari AC (2007) Raman spectroscopy of graphene and graphite: disorder, electron–phonon coupling, doping and nonadiabatic effects. *Solid State Commun.* <https://doi.org/10.1016/j.ssc.2007.03.052>
58. Dresselhaus MS, Dresselhaus G, Hofmann M (2008) Raman spectroscopy as a probe of graphene and carbon nanotubes. *Philos Trans A Math Phys Eng Sci.* <https://doi.org/10.1098/rsta.2007.2155>
59. Casiraghi C, Hartschuh A, Qian H, Piscanec S, Georgi C, Fasoli A, Novoselov KS, Basko DM, Ferrari AC (2009) Raman spectroscopy of graphene edges. *Nano Lett.* <https://doi.org/10.1021/nl8032697>
60. Kim YA, Fujisawa K, Muramatsu H, Hayashi T, Endo M, Fujimori T, Kaneko K, Terrones M, Behrends J, Eckmann A, Casiraghi C, Novoselov KS, Saito R, Dresselhaus MS (2012) Raman spectroscopy of boron-doped single-layer graphene. *ACS Nano.* <https://doi.org/10.1021/nn301728j>
61. Ferrari AC, Basko DM (2013) Raman spectroscopy as a versatile tool for studying the properties of graphene. *Nat Nanotechnol.* <https://doi.org/10.1038/nnano.2013.46>
62. Kumar J, Ansh, and Shrivastava M, (2020) Stone-wales defect and vacancy-assisted enhanced atomic orbital interactions between graphene and ambient gases: a first-principles insight. *ASC Omega.* <https://doi.org/10.1021/acsomega.0c04729>
63. Qi JL, Wang X, Lin JH, Zhang F, Feng JC, Fei WD (2015) A high-performance supercapacitor of vertically-oriented few-layered graphene with high-density defects. *Nanoscale.* <https://doi.org/10.1039/c4nr07284g>
64. Johra FT, Lee JW, Jung WG (2014) Facile and safe graphene preparation on solution based platform. *J Ind Eng Chem.* <https://doi.org/10.1016/j.jiec.2013.11.022>
65. Torrisi L, Silipigni L, Cutroneo M, Torrisi A (2020) Graphene oxide as a radiation sensitive material for XPS dosimetry. *Vacuum.* <https://doi.org/10.1016/j.vacuum.2020.109175>
66. Rabchinskii MK, Dideikin AT, Kirilenko DA, Baidakova MV, Shnitov VV, Roth F, Konyakhin SV, Besedina NA, Pavlov SI, Kuricyn RA, Lebedeva NM, Brunkov PN, Vul' AY (2018) Facile reduction of graphene oxide suspensions and films using glass wafers. *Sci Rep.* <https://doi.org/10.1038/s41598-018-32488-x>
67. Çiplak Z, Yildiz N, Çalimli A (2015) Investigation of graphene/Ag nanocomposites synthesis parameters for two different synthesis Methods. *Fuller Nanotub Carbon Nanostruct.* <https://doi.org/10.1080/1536383x.2014.894025>
68. Surekha G, Krishnaiah KV, Ravi N, Padma Suvarna R (2020) FTIR, Raman and XRD analysis of graphene oxide films prepared by modified Hummers method. *J Phys Conf Ser.* <https://doi.org/10.1088/1742-6596/1495/1/012012>
69. Aragaw BA (2020) Reduced graphene oxide-intercalated graphene oxide nano-hybrid for enhanced photoelectrochemical water reduction. *J Nanostruct ure Chem.* <https://doi.org/10.1007/s40097-019-00324-x>
70. Saleem H, Haneef M, Abbasi HY (2018) Synthesis route of reduced graphene oxide via thermal reduction of chemically exfoliated graphene oxide. *Mater Chem Phys.* <https://doi.org/10.1016/j.matchemphys.2017.10.020>
71. Al-Gaashani R, Najjar A, Zakaria Y, Mansour S, Atieh MA (2019) XPS and structural studies of high quality graphene oxide and reduced graphene oxide prepared by different chemical oxidation methods. *Ceram Int.* <https://doi.org/10.1016/j.ceramint.2019.04.165>
72. Paredes JI, Villar-Rodil S, Solís-Fernández P, Martínez-Alonso A, Tascón JMD (2009) Atomic force and scanning tunneling microscopy imaging of graphene nanosheets derived from graphite oxide. *Langmuir.* <https://doi.org/10.1021/la804216z>
73. Gammelgaard L, Caridad JM, Cagliani A, Mackenzie PDH, Booth TJ, Bøggild P (2014) Graphene transport properties upon exposure to PMMA processing and heat treatments. *2D Mater.* <https://doi.org/10.1088/2053-1583/1/3/035005>
74. Dubin S, Gilje S, Wang K, Tung VC, Cha K, Hall AS, Farrar J, Varshneya R, Yang Y, Kaner RB (2010) A one-step, solvothermal reduction method for producing reduced graphene oxide dispersions in organic solvents. *ACS Nano.* <https://doi.org/10.1021/nn100511a>
75. Chen C, Yang Q-H, Yang Y, Lv W, Wen Y, Hou P-X, Wang M, Cheng H-M (2009) Self-assembled free-standing graphite oxide membrane. *Adv Mater.* <https://doi.org/10.1002/adma.200803726>
76. Dikin DA, Stankovich S, Zimney EJ, Piner RD, Dommett GHB, Evmenenko G, Nguyen ST, Ruoff RS (2007) Preparation and characterization of graphene oxide paper. *Nature.* <https://doi.org/10.1038/nature06016>
77. Azizighannad S, Mitra S (2018) Stepwise reduction of graphene oxide (GO) and its effects on chemical and colloidal properties. *Sci Rep.* <https://doi.org/10.1038/s41598-018-28353-6>
78. Lovén K, Franzén SM, Isaxon C, Messing ME, Martinsson J, Gudmundsson A, Pagels J, Hedmer M, NanoLund (2021) Emissions and exposures of graphene nanomaterials, titanium dioxide nanofibers, and nanoparticles during down-stream industrial handling. *J Expo Sci Environ Epidemiol.* <https://doi.org/10.1038/s41370-020-0241-3>
79. Qian L, Thirupathi AR, Elmahdy R, van der Zalm J, Chen A (2020) Graphene-oxide-based electrochemical sensors for the sensitive detection of pharmaceutical drug naproxen. *Sensors.* <https://doi.org/10.3390/s20051252>
80. Gómez-Navarro C, Meyer JC, Sundaram RS, Chuvilin A, Kurasch S, Burghard M, Kern K, Kaiser U (2010) Atomic structure of reduced graphene oxide. *Nano Lett.* <https://doi.org/10.1021/nl9031617>
81. Szabo T, Maroni P, Szilagyi I (2020) Size-dependent aggregation of graphene oxide. *Carbon.* <https://doi.org/10.1016/j.carbon.2020.01.022>
82. Konkana B, Vasudevan S (2012) Understanding aqueous dispersibility of graphene oxide and reduced graphene oxide through pKa measurements. *J Phys Chem Lett.* <https://doi.org/10.1021/jz300236w>
83. Park WK, Yoon Y, Kim S, Choi SY, Yoo S, Do Y, Jung S, Yoon DH, Park H, Yang WS (2017) Toward green synthesis of graphene oxide using recycled sulfuric acid via Couette–Taylor flow. *ACS Omega.* <https://doi.org/10.1021/acsomega.6b00352>
84. Priyadarsini S, Mohanty S, Mukherjee S, Basu S, Mishra M (2018) Graphene and graphene oxide as nanomaterials for medicine and biology application. *J Nanostruct Chem.* <https://doi.org/10.1007/s40097-018-0265-6>

85. Raccichini R, Varzi A, Passerini S, Scrosati B (2015) The role of graphene for electrochemical energy storage. *Nat Mater*. <https://doi.org/10.1038/nmat4170>
86. Velasco A, Ryu YK, Boscá A, Ladrón-de-Guevara A, Hunt E, Zuo J, Pedrós J, Calle F, Martínez J (2021) Recent trends in graphene supercapacitors: from large area to microsupercapacitors. *Sustain Energy Fuels*. <https://doi.org/10.1039/d0se01849j>
87. Grande L, Chundi VT, Wei D, Bower C, Andrew P, Ryhänen T (2012) Graphene for energy harvesting/storage devices and printed electronics. *Particuology*. <https://doi.org/10.1016/j.partic.2011.12.001>
88. Lü M, Li J, Yang X, Zhang C, Yang J, Hu H, Wang X (2013) Applications of graphene-based materials in environmental protection and detection. *Chin Sci Bull*. <https://doi.org/10.1007/s11434-013-5887-y>
89. Liang J, Wang Y, Huang Y, Ma Y, Liu Z, Cai J, Zhang C, Gao H, Chen Y (2009) Electromagnetic interference shielding of graphene/epoxy composites. *Carbon*. <https://doi.org/10.1016/j.carbon.2008.12.038>
90. Lovat G (2012) Equivalent circuit for electromagnetic interaction and transmission through graphene sheets. *IEEE Trans Electromagn*. <https://doi.org/10.1109/TEMC.2011.2169072>
91. Hong SK, Kim KY, Kim TY, Kim JH, Park SW, Kim JH, Cho BJ (2012) Electromagnetic interference shielding effectiveness of monolayer graphene. *Nanotechnology*. <https://doi.org/10.1088/0957-4484/23/45/455704>
92. Lu Z, Ma L, Tan J, Wang H, Ding X (2016) Transparent multilayer graphene/polyethylene terephthalate structures with excellent microwave absorption and electromagnetic interference shielding performance. *Nanoscale*. <https://doi.org/10.1039/c6nr02619b>
93. Dresselhaus MS, Jorio A, Souza Filho AG, Saito R (2010) Defect characterization in graphene and carbon nanotubes using Raman spectroscopy. *Philos Trans A Math Phys Eng Sci*. <https://doi.org/10.1098/rsta.2010.0213>
94. Zhang L, Alvarez NT, Zhang M, Haase M, Malik R, Mast D, Shanov V (2015) Preparation and characterization of graphene paper for electromagnetic interference shielding. *Carbon*. <https://doi.org/10.1016/j.carbon.2014.10.080>
95. Paliotta L, De Bellis G, Tamburrano A, Marra F, Rinaldi A, Balijepalli SK, Kaciulis S, Sarto MS (2015) Highly conductive multilayer-graphene paper as a flexible lightweight electromagnetic shield. *Carbon*. <https://doi.org/10.1016/j.carbon.2015.03.043>
96. Lin S, Ju S, Zhang J, Shi G, He Y, Jiang D (2019) Ultrathin flexible graphene films with high thermal conductivity and excellent EMI shielding performance using large-sized graphene oxide flakes. *RSC Adv*. <https://doi.org/10.1039/C8RA09376H>
97. Liu X, Wu W, Guo B, Cui M, Ma H, Zhang Z, Zhang R (2021) Facile fabrication of ultrathin graphene film with ultrahigh electrical conductivity and superb electromagnetic interference shielding effectiveness. *J Mater Chem C*. <https://doi.org/10.1039/D0TC04576D>
98. Wan YJ, Zhu PL, Yu SH, Sun R, Wong C, Liao WH (2017) Graphene paper for exceptional EMI shielding performance using large-sized graphene oxide sheets and doping strategy. *Carbon*. <https://doi.org/10.1016/j.carbon.2017.06.042>
99. Shahzad F, Kumar P, Kim YH, Hong SM, Koo CM (2016) Biomass-derived thermally annealed interconnected sulfur-doped graphene as a shield against electromagnetic interference. *ACS Appl Mater Interfaces*. <https://doi.org/10.1021/acsami.6b00418>
100. Shahzad F, Kumar P, Yu S, Lee S, Kim YH, Hong SM, Koo CM (2015) Sulfur-doped graphene laminates for EMI shielding applications. *J Mater Chem C*. <https://doi.org/10.1039/C5TC02166A>
101. Lin S, Ju S, Shi G, Zhang J, He Y, Jiang D (2019) Ultrathin nitrogen-doping graphene films for flexible and stretchable EMI shielding materials. *J Mater Sci*. <https://doi.org/10.1007/s10853-019-03372-4>
102. Yutomo EB, Noor FA, Winata T (2021) Effect of the number of nitrogen dopants on the electronic and magnetic properties of graphitic and pyridinic N-doped graphene—a density-functional study. *RSC Adv*. <https://doi.org/10.1039/d1ra01095f>
103. Zhang Y, Fu Y, Mao Q, Zhang G, Zhang W, Wang Y, Yang W (2022) First-principle calculation of electronic structure and optical properties of (P, Ga, P–Ga) doped graphene. *Open Phys*. <https://doi.org/10.1515/phys-2022-0061>
104. Zhang Y, Zhang G, Shi X, Gao Q, Huang F, Xiao R (2021) A flexible and strong reduced graphene oxide film for high-performance electromagnetic shielding. *Compos Commun*. <https://doi.org/10.1016/j.coco.2021.100954>
105. Eswaraiyah V, Sankaranarayanan V, Ramaprabhu S (2011) Functionalized graphene–PVDF foam composites for EMI shielding. *Macromol Mater Eng*. <https://doi.org/10.1002/mame.201100035>
106. Oliveira FM, Luxa J, Bouša D, Sofer Z, Gusmão R (2022) Electromagnetic interference shielding by reduced graphene oxide foils. *ACS Appl Nano Mater*. <https://doi.org/10.1021/acsanm.2c00785>
107. Huang M, Wang C, Quàn L, Nguyen T, Zhang H, Jiang Y, Byun G, Ruoff R (2020) CVD growth of porous graphene foam in film form. *Matter*. <https://doi.org/10.1016/j.matt.2020.06.012>
108. Chen C, Zhao Y, Wei W, Tao J, Lei G, Jia D, Wan M, Li S, Ji S, Ye C (2017) Fabrication of silver nanowire transparent conductive films with an ultra-low haze and ultra-high uniformity and their application in transparent electronics. *J Mater Chem C*. <https://doi.org/10.1039/c6tc05455b>
109. Gerlein LF, Benavides-Guerrero JA, Cloutier SG (2021) High-performance silver nanowires transparent conductive electrodes fabricated using manufacturing-ready high-speed photonic sinterization solutions. *Sci Rep*. <https://doi.org/10.1038/s41598-021-03528-w>
110. Wang P, Jian M, Wu M, Zhang C, Zhou C, Ling X, Zhang J, Yang L (2022) Highly sandwich-structured silver nanowire hybrid transparent conductive films for flexible transparent heater applications. *Compos Part A Appl Sci*. <https://doi.org/10.1016/j.compositesa.2022.106998>
111. Jiu J, Sugahara T, Nogi M, Nagao S, Suganuma K (2013) Silver nanowires transparent conductive films: fabrication using different sintering techniques. In: 2013 13th IEEE international conference on nanotechnology (IEEE-NANO 2013).
112. De S, Higgins TM, Lyons PE, Doherty EM, Nirmalraj PN, Blau WJ, Boland JJ, Coleman JN (2009) Silver nanowire networks as flexible, transparent, conducting films extremely high DC to optical conductivity ratios. *ACS Nano*. <https://doi.org/10.1021/nn900348c>
113. Amjadi M, Pichitpajongkit A, Lee S, Ryu S, Park I (2014) Highly stretchable and sensitive strain sensor based on silver nanowire-elastomer nanocomposite. *ACS Nano*. <https://doi.org/10.1021/nn501204t>
114. Chae WH, Sannicò T, Grossman JC (2020) Double-sided graphene oxide encapsulated silver nanowire transparent electrode with improved chemical and electrical stability. *ACS Appl Mater Interfaces*. <https://doi.org/10.1021/acsami.0c03587>
115. Wu C, Fang L, Huang X, Jiang P (2014) Three-dimensional highly conductive graphene-silver nanowire hybrid foams for flexible and stretchable conductors. *ACS Appl Mater Interfaces*. <https://doi.org/10.1021/am505908d>
116. Qian F, Lan PC, Freyman MC, Chen W, Kou T, Olson TY, Zhu C, Worsley MA, Duoss EB, Spadaccini CM, Baumann T, Han

- TYJ (2017) Ultralight conductive silver nanowire aerogels. *Nano Lett.* <https://doi.org/10.1021/acs.nanolett.7b02790>
117. Lu Y, Jiang J, Yoon S, Kim KS, Kim JH, Park S, Kim SH, Piao L (2018) High-performance stretchable conductive composite fibers from surface-modified silver nanowires and thermoplastic polyurethane by wet spinning. *ACS Appl Mater Interfaces.* <https://doi.org/10.1021/acsami.7b16022>
 118. Fortin E, Weichman FL (1964) Photoconductivity in Ag_2O . *Phys Status Solidi B.* <https://doi.org/10.1002/pssb.19640050308>
 119. Mayousse C, Celle C, Fraczkiewicz A, Simonato JP (2015) Stability of silver nanowire based electrodes under environmental and electrical stresses. *Nanoscale.* <https://doi.org/10.1039/c4nr06783e>
 120. Graedel TE (1992) Corrosion mechanisms for silver exposed to the atmosphere. *J Electrochem Soc* doi 10(1149/1):2221162
 121. Franey JP, Kammlott GW, Graedel TE (1985) The corrosion of silver by atmospheric sulfurous gases. *Corros Sci.* [https://doi.org/10.1016/0010-938X\(85\)90104-0](https://doi.org/10.1016/0010-938X(85)90104-0)
 122. Hebb MH (2004) Electrical conductivity of silver sulfide. *J Chem Phys.* <https://doi.org/10.1063/1.1700165>
 123. Zhang Y, Bai S, Chen T, Yang H, Guo X (2020) Facile preparation of flexible and highly stable graphene oxide-silver nanowire hybrid transparent conductive electrode. *Mater Res Express.* <https://doi.org/10.1088/2053-1591/ab6262>
 124. Hu M, Gao J, Dong Y, Li K, Shan G, Yang S, Li RKY (2012) Flexible transparent PES/silver nanowires/PET sandwich-structured film for high-efficiency electromagnetic interference shielding. *Langmuir.* <https://doi.org/10.1021/la300720y>
 125. Yu YH, Ma CCM, Teng CC, Huang YL, Lee SH, Wang I, Wei MH (2012) Electrical, morphological, and electromagnetic interference shielding properties of silver nanowires and nanoparticles conductive composites. *Mater Chem Phys.* <https://doi.org/10.1016/j.matchemphys.2012.05.024>
 126. Fang F, Li YQ, Xiao HM, Hu N, Fu SY (2016) Layer-structured silver nanowire/polyaniline composite film as a high performance X-band EMI shielding material. *J Mater Chem C* 4:4193–4203. <https://doi.org/10.1039/c5tc04406e>
 127. Wan YJ, Zhu PL, Yu SH, Sun R, Wong CP, Liao WH (2018) Anticorrosive, ultralight, and flexible carbon-wrapped metallic nanowire hybrid sponges for highly efficient electromagnetic interference shielding. *Small.* <https://doi.org/10.1002/sml.20180534>
 128. Jia LC, Ding KQ, Ma RJ, Wang HL, Sun WJ, Yan DX, Li B, Li ZM (2019) Highly conductive and machine-washable textiles for efficient electromagnetic interference shielding. *Adv Mater Technol.* <https://doi.org/10.1002/admt.201800503>
 129. Liu LX, Chen W, Zhang HB, Wang QW, Guan F, Yu ZZ (2019) Flexible and multifunctional silk textiles with biomimetic leaf-like MXene/silver nanowire nanostructures for electromagnetic interference shielding, humidity monitoring, and self-derived hydrophobicity. *Adv Funct Mater.* <https://doi.org/10.1002/adfm.201905197>
 130. Zhou B, Su M, Yang D, Han G, Feng Y, Wang B, Ma J, Liu C, Shen C (2020) Flexible MXene/silver nanowire-based transparent conductive film with electromagnetic interference shielding and electro-photo-thermal performance. *ACS Appl Mater Interfaces.* <https://doi.org/10.1021/acsami.0c09020>
 131. Chen W, Liu LX, Zhang HB, Yu ZZ (2020) Flexible transparent, and conductive $\text{Ti}_3\text{C}_2\text{T}_x$ MXene-silver nanowire films with smart acoustic sensitivity for high-performance electromagnetic interference shielding. *ACS Nano.* <https://doi.org/10.1021/acsnano.0c01635>
 132. Cheng Y, Lu Y, Xia M, Piao L, Liu Q, Li M, Zhou Y, Jia K, Yang L, Wang D (2021) Flexible and lightweight MXene/silver nanowire/polyurethane composite foam films for highly efficient electromagnetic interference shielding and photothermal conversion. *Compos Sci Technol.* <https://doi.org/10.1016/j.compscitech.2021.109023>
 133. Liu J, Zhang Y, Cheng W, Lei S, Song L, Wang B, Hu Y (2022) Anti-fogging, frost-resistant transparent and flexible silver nanowire- $\text{Ti}_3\text{C}_2\text{T}_x$ MXene based composite films for excellent electromagnetic interference shielding ability. *J Colloid Interface Sci.* <https://doi.org/10.1016/j.jcis.2021.10.171>
 134. Ma Z, Feng H, Feng Y, Ding X, Wang X, Wang W, Zhang X, Kong S, Lan X, Li Q (2022) An ultralight and thermally conductive $\text{Ti}_3\text{C}_2\text{T}_x$ MXene-silver nanowire cellular composite film for high-performance electromagnetic interference shielding. *J Mater Chem C.* <https://doi.org/10.1039/d2tc02856e>
 135. Liu J, Lin S, Huang K, Jia C, Wang Q, Li Z, Song J, Liu Z, Wang H, Lei M, Wu H (2020) A large-area AgNW-modified textile with high-performance electromagnetic interference shielding. *npj Flex Electron.* <https://doi.org/10.1038/s41528-020-0074-0>
 136. Yang S, Wang YY, Song YN, Jia LC, Zhong GJ, Xu L, Yan DX, Lei J, Li ZM (2021) Ultrathin, flexible and sandwich-structured PHBV/silver nanowire films for high-efficiency electromagnetic interference shielding. *J Mater Chem C.* <https://doi.org/10.1039/d0tc05266c>
 137. Hong W, Sun B, Li Z, Fu Z, Zhang J, Jiang M, Zhang Y, Li Y, Qian K (2022) Biodegradable, Flexible Transparent Ordered Ag NWs Micromesh Conductor for Electrical Heater and Electromagnetic Interference Shielding Applications. *ACS Appl Electron Mater.* <https://doi.org/10.1021/acsaelm.2c01109>
 138. Zhang F, Hu J, Zhao P, He P, Mi HY, Guo Z, Liu C, Shen C (2021) Multifunctional electromagnetic interference shielding films comprised of multilayered thermoplastic polyurethane membrane and silver nanowire. *Compos Part A Appl Sci.* <https://doi.org/10.1016/j.compositesa.2021.106472>
 139. Huang X, Wang L, Shen Z, Ren J, Chen G, Li Q, Zhou Z (2022) Super-stretchable and self-healing hydrogel with a three-dimensional silver nanowires network structure for wearable sensor and electromagnetic interference shielding. *J Chem Eng.* <https://doi.org/10.1016/j.cej.2022.137136>
 140. Zhang X, Shan J, Liu C, Li Z, Guo X, Zhao X, Yang H (2022) High corrosion-resistant silver nanowire/poly(3,4-ethylene dioxithiophene)/poly(styrene sulfonate)@nickel electrode for transparent electromagnetic shielding film. *J Mater.* <https://doi.org/10.1016/j.jmat.2022.05.008>
 141. Zhang B, Liu D, Liang Y, Zhang D, Yan H, Zhang Y (2017) Flexible transparent and conductive films of reduced-graphene-oxide wrapped silver nanowires. *Mater Lett.* <https://doi.org/10.1016/j.matlet.2017.04.137>
 142. Liu X, Chen T, Liang H, Qin F, Yang H, Guo X (2019) Facile approach for a robust graphene/silver nanowires aerogel with high-performance electromagnetic interference shielding. *RSC Adv.* <https://doi.org/10.1039/C8RA08738E>
 143. Yan S, Li P, Ju Z, Chen H, Ma J (2021) Electromagnetic interference shielding performance enhancement of stretchable transparent conducting silver nanowire networks with graphene encapsulation. *J Mater Sci Mater Electron.* <https://doi.org/10.1007/s10854-021-06096-x>
 144. Jia H, Yi YL, Huang XH, Su FY, Kong QQ, Yang X, Wang Z, Xie LJ, Guo QG, Chen CM (2021) A one-step graphene induction strategy enables in-situ controllable growth of silver nanowires for electromagnetic interference shielding. *Carbon.* <https://doi.org/10.1016/j.carbon.2021.07.067>
 145. Giasafaki D, Mitzithra C, Belessi V, Filippakopoulou T, Koutsoukis A, Georgakilas V, Charalambopoulou G, Steriotis T (2022) Graphene-based composites with silver nanowires for electronic applications nanomaterials. *Nanomaterials.* <https://doi.org/10.3390/nano12193443>
 146. Łapińska A, Grochowska N, Filak K, Michalski P, Szymański KR, Zaleski PA, Dydek K, Daniszewska A, Żerańska K,

- Dużyńska A, Kowalczyk S, Plichta A (2023) Non-metallic multifunctional PVDF – graphene nanoplatelets nanocomposites as an effective electromagnetic shield, thermal and electrical conductor. *Mater Today Adv.* <https://doi.org/10.1016/j.mtadv.2023.100365>
147. Mutlu G, Yildirim F, Ulus H, Eskizeybek V (2023) Coating graphene nanoplatelets onto carbon fabric with controlled thickness for improved mechanical performance and EMI shielding effectiveness of carbon/epoxy composites. *Eng Fract Mech.* <https://doi.org/10.1016/j.engfracmech.2023.109271>
148. Wu C, Zeng L, Chang G, Zhou Y, Yan K, Xie L, Xue B, Zheng Q (2023) Composite phase change materials embedded into cellulose/polyacrylamide/graphene nanosheets/silver nanowire hybrid aerogels simultaneously with effective thermal management and anisotropic electromagnetic interference shielding. *Adv Compos Hybrid Mater.* <https://doi.org/10.1007/s42114-022-00618-9>
149. Zhang F, Ren P, Guo H, Zhang Z, Guo Z, Dai Z, Lu Z, Jin Y, Ren F (2021) Flexible and conductive cellulose composite paper for highly efficient electromagnetic interference shielding. *Adv Electron Mater.* <https://doi.org/10.1002/aelm.202100496>
150. Zhu M, Yan X, Li X, Dai L, Guo J, Lei Y, Xu Y, Xu H (2022) Flexible, transparent, and hazy composite cellulosic film with interconnected silver nanowire networks for EMI shielding and joule heating. *ACS Appl Mater Interfaces.* <https://doi.org/10.1021/acami.2c13035>
151. Hu G, Wu C, Wang Q, Dong F, Xiong Y (2022) Ultrathin nanocomposite films with asymmetric gradient alternating multilayer structures exhibit superhigh electromagnetic interference shielding performances and robust mechanical properties. *J Chem Eng.* <https://doi.org/10.1016/j.cej.2022.137537>
152. Nimbalkar P, Korde A, Goyal RK (2018) Electromagnetic interference shielding of polycarbonate/GNP nanocomposites in X-band. *Mater Chem Phys.* <https://doi.org/10.1016/j.matchemphys.2017.12.027>
153. Wang Y, Jing X (2005) Intrinsically conducting polymers for electromagnetic interference shielding. *Polym Adv Technol.* <https://doi.org/10.1002/pat.589>
154. Sushmita K, Madras G, Bose S (2021) The journey of polycarbonate-based composites towards suppressing electromagnetic radiation. *Funct Compos Mater.* <https://doi.org/10.1186/s42252-021-00025-1>
155. Cao M, Lian H, Hu C (2010) Ligand-assisted fabrication of hollow CdSe nanospheres via Ostwald ripening and their microwave absorption properties. *Nanoscale.* <https://doi.org/10.1039/c0nr00674b>
156. Valenzuela M, Bosch P, Jiménez-Becerrill J, Quiroz O, Páez A (2002) Preparation, characterization and photocatalytic activity of ZnO, Fe₂O₃ and ZnFe₂O₄. *J Photochem Photobiol A.* [https://doi.org/10.1016/S1010-6030\(02\)00040-0](https://doi.org/10.1016/S1010-6030(02)00040-0)
157. Menon AV, Madras G, Bose S (2019) Mussel-inspired self-healing polyurethane with “flower-like” magnetic MoS₂ as efficient microwave absorbers. *ACS Appl Polym Mater.* <https://doi.org/10.1021/acsp.9b00538>
158. Moučka R, Sedláčik M, Prokeš J, Kasparyan H, Valtera S, Kopecký D (2020) Electromagnetic interference shielding of polypyrrole nanostructures. *Synt Met.* <https://doi.org/10.1016/j.synthmet.2020.116573>
159. Dabas S, Chahar M, Thakur OP (2022) Electromagnetic interference shielding properties of CoFe₂O₄/polyaniline/poly(vinylidene fluoride) nanocomposites. *Mater Chem Phys.* <https://doi.org/10.1016/j.matchemphys.2021.125579>
160. Zubair K, Ashraf A, Gulzar H, Shakir MF, Nawab Y, Rehan ZA, Rashid IA (2021) Study of mechanical, electrical and EMI shielding properties of polymer-based nanocomposites incorporating polyaniline coated graphene nanoparticles. *Nano Express.* <https://doi.org/10.1088/2632-959X/abe843>
161. Awad EH, El-Nemr KF, Atta MM, Abdel-Hakim A, Sharaf A (2023) Electromagnetic interference shielding efficiency of irradiated wood-plastic composites based on graphene oxide nanoparticles. *Radiat Phys Chem.* <https://doi.org/10.1016/j.radphyschem.2022.110629>
162. Kim S, Oh JS, Kim MG, Jang W, Wang M, Kim Y, Seo HW, Kim YC, Lee JH, Lee Y, Nam JD (2014) Electromagnetic interference (EMI) transparent shielding of reduced graphene oxide (RGO) interleaved structure fabricated by electrophoretic deposition. *ACS Appl Mater Interfaces* 6:17647–17653. <https://doi.org/10.1021/am503893v>
163. Batrakov K, Kuzhir P, Maksimenko S, Paddubskaya A, Voronovich S, Lambin P, Kaplas T, Svirko Y (2014) Flexible transparent graphene/polymer multilayers for efficient electromagnetic field absorption. *Sci Report.* <https://doi.org/10.1038/srep07191>
164. Han Y, Liu Y, Han L, Lin J, Jin P (2017) High-performance hierarchical graphene/metal-mesh film for optically transparent electromagnetic interference shielding. *Carbon.* <https://doi.org/10.1016/j.carbon.2016.12.092>
165. Tran VV, Nguyen DD, Nguyen TA, Hofmann M, Hsieh YP, Kan HC, Hsu CC (2020) Electromagnetic interference shielding by transparent graphene/nickel mesh films. *ACS Appl Nano Mater.* <https://doi.org/10.1021/acsnm.0c01076>
166. Ray B, Parmar S, Date K, Datar S (2021) Optically transparent polymer composites: a study on the influence of filler/dopant on electromagnetic interference shielding mechanism. *J Appl Polym Sci.* <https://doi.org/10.1002/app.50255>
167. Bai S, Guo X, Zhang X, Zhao X, Yang H (2021) Ti₃C₂T_x MXene–AgNW composite flexible transparent conductive films for EMI shielding. *Compos Part A Appl Sci.* <https://doi.org/10.1016/j.compositesa.2021.106545>
168. Reis FCD, Rezende MC, Ribeiro B (2021) The influence of the transparent layer thickness on the absorption capacity of epoxy/carbon nanotube buckypaper at X-band. *J Appl Polym Sci.* <https://doi.org/10.1002/app.51407>
169. Shi K, Su J, Liang H, Hu K, Xu J (2022) Highly optically transparent graphene mesh for electromagnetic interference shielding. *Diam Relat Mater.* <https://doi.org/10.1016/j.diamond.2022.108849>
170. Wang G, Zhao Y, Yang F, Zhang Y, Zhou M, Ji G (2022) Multifunctional integrated transparent film for efficient electromagnetic protection. *Nano-Micro Lett.* <https://doi.org/10.1007/s40820-022-00810-y>

Publisher's Note Springer Nature remains neutral with regard to jurisdictional claims in published maps and institutional affiliations.